



Reconstruction of secular variation in seawater sulfate concentrations

T. J. Algeo^{1,2,3}, G. M. Luo¹, H. Y. Song², T. W. Lyons⁴, and D. E. Canfield⁵

¹State Key Laboratory of Geological Processes and Mineral Resources, China University of Geosciences, Wuhan, 430074, China

²State Key Laboratory of Biogeology and Environmental Geology, China University of Geosciences, Wuhan, 430074, China

³Department of Geology, University of Cincinnati, Cincinnati, Ohio 45221-0013, USA

⁴Department of Earth Sciences, University of California, Riverside, California 92521-0423, USA

⁵Nordic Center for Earth Evolution (NordCEE) and Institute of Biology, University of Southern Denmark, Campusvej 55, 5230 Odense M, Denmark

Correspondence to: T. J. Algeo (thomas.algeo@uc.edu)

Received: 26 July 2014 – Published in Biogeosciences Discuss.: 10 September 2014

Revised: 24 January 2015 – Accepted: 18 March 2015 – Published: 10 April 2015

Abstract. Long-term secular variation in seawater sulfate concentrations ($[\text{SO}_4^{2-}]_{\text{SW}}$) is of interest owing to its relationship to the oxygenation history of Earth's surface environment. In this study, we develop two complementary approaches for quantification of sulfate concentrations in ancient seawater and test their application to late Neoproterozoic (635 Ma) to Recent marine units. The “rate method” is based on two measurable parameters of paleomarine systems: (1) the S-isotope fractionation associated with microbial sulfate reduction (MSR), as proxied by $\Delta^{34}\text{S}_{\text{CAS-PY}}$, and (2) the maximum rate of change in seawater sulfate, as proxied by $\partial\delta^{34}\text{S}_{\text{CAS}}/\partial t(\text{max})$. The “MSR-trend method” is based on the empirical relationship of $\Delta^{34}\text{S}_{\text{CAS-PY}}$ to aqueous sulfate concentrations in 81 modern depositional systems. For a given paleomarine system, the rate method yields an estimate of maximum possible $[\text{SO}_4^{2-}]_{\text{SW}}$ (although results are dependent on assumptions regarding the pyrite burial flux, F_{PY}), and the MSR-trend method yields an estimate of mean $[\text{SO}_4^{2-}]_{\text{SW}}$. An analysis of seawater sulfate concentrations since 635 Ma suggests that $[\text{SO}_4^{2-}]_{\text{SW}}$ was low during the late Neoproterozoic (< 5 mM), rose sharply across the Ediacaran–Cambrian boundary (~ 5 – 10 mM), and rose again during the Permian (~ 10 – 30 mM) to levels that have varied only slightly since 250 Ma. However, Phanerozoic seawater sulfate concentrations may have been drawn down to much lower levels (~ 1 – 4 mM) dur-

ing short ($< \sim 2$ Myr) intervals of the Cambrian, Early Triassic, Early Jurassic, and Cretaceous as a consequence of widespread ocean anoxia, intense MSR, and pyrite burial. The procedures developed in this study offer potential for future high-resolution quantitative analyses of paleo-seawater sulfate concentrations.

1 Introduction

Oceanic sulfate plays a key role in the biogeochemical cycles of S, C, O, and Fe (Canfield, 1998; Lyons and Gill, 2010; Halevy et al., 2012; Planavsky et al., 2012). For example, $> 50\%$ of organic matter and methane in marine sediments is oxidized via processes linked to microbial sulfate reduction (MSR) (Jørgensen, 1982; Valentine, 2002). At a concentration of ~ 29 mM in the modern ocean, sulfate is the second most abundant anion in seawater (Millero, 2005). Its concentration is an important proxy for seawater chemistry and the oxidation state of the Earth's atmosphere and oceans (Kah et al., 2004; Johnston, 2011).

Although there is broad agreement that seawater sulfate concentrations have increased through time, the history of its accumulation remains poorly known in detail. Archean and Early Proterozoic oceans are thought to have had very limited sulfate inventories (< 200 μM), as implied by small

degrees of sulfate–sulfide and mass-independent S-isotope fractionation (Shen et al., 2001; Strauss, 2003; Farquhar et al., 2007; Adams et al., 2010; Johnston, 2011; Owens et al., 2013; Luo et al., 2015). The accumulation of atmospheric O₂ during the “Great Oxidation Event” (~2.3–2.0 Ga; Holland, 2002; Bekker et al., 2004) is thought to have resulted in a long-term increase in seawater sulfate concentrations (Canfield and Raiswell, 1999; Canfield et al., 2007; Kah et al., 2004; Fike et al., 2006). However, this increase was probably not monotonic and declines in *p*O₂ may have resulted in one or more seawater sulfate minima between ~1.9 and 0.6 Ga (Planavsky et al., 2012; Luo et al., 2015). Estimates of Phanerozoic seawater sulfate concentrations are uniformly higher, although there is no consensus regarding exact values. Fluid inclusion data yielded estimates of ~10 to 30 mM for most of the Phanerozoic (Horita et al., 2002; Lowenstein et al., 2003, 2005). However, recent S-isotope studies have modeled concentrations as low as ~1–5 mM during portions of the Cambrian, Triassic, Jurassic, and Cretaceous (Wortmann and Chernyavsky, 2007; Adams et al., 2010; Luo et al., 2010; Gill et al., 2011a, b; Newton et al., 2011; Owens et al., 2013; Song et al., 2014), and a recent marine S-cycle model yielded low concentrations (< 10 mM) for much of the Cretaceous and early Cenozoic before a rise to near-modern levels at ~40 Ma (Wortmann and Paytan, 2012).

Here, we develop two approaches for quantitative analysis of seawater sulfate concentrations ($[\text{SO}_4^{2-}]_{\text{SW}}$) in paleomarine systems. The first method calculates a maximum possible $[\text{SO}_4^{2-}]_{\text{SW}}$ based on a combination of two parameters that are readily measurable in most paleomarine systems: (1) the S-isotope fractionation between co-genetic sedimentary sulfate and sulfide ($\Delta^{34}\text{S}_{\text{CAS-PY}}$), and (2) the maximum observed rate of variation in seawater sulfate $\delta^{34}\text{S}$ ($\partial\delta^{34}\text{S}_{\text{CAS}}/\partial t$). This rate-based method is an extension of earlier modeling work by Kump and Arthur (1999), Kurtz et al. (2003), Kah et al. (2004), Bottrell and Newton (2006), and Gill et al. (2011a, b). The second approach yields an estimate of mean seawater $[\text{SO}_4^{2-}]$ based on an empirical relationship between $\Delta^{34}\text{S}_{\text{CAS-PY}}$ and aqueous sulfate concentrations (the “MSR trend”) in 81 modern depositional systems. Conceptually, the MSR-trend method is related to the fractionation relationship given in Habicht et al. (2002, their Fig. 1). Although some earlier studies have made qualitative assessments of paleo-seawater $[\text{SO}_4^{2-}]$, the significance of our methodology is that the $[\text{SO}_4^{2-}]$ of ancient seawater can be quantitatively constrained as a function of measurable sediment parameters and empirical fractionation relationships.

We fully recognize that the marine sulfur cycle is controlled by myriad factors, many of which are only now coming to light thanks to detailed field and laboratory studies, and that not all such influences can be thoroughly considered and accommodated in the present study. While acknowledging the complexity of the sulfur cycle, this study attempts

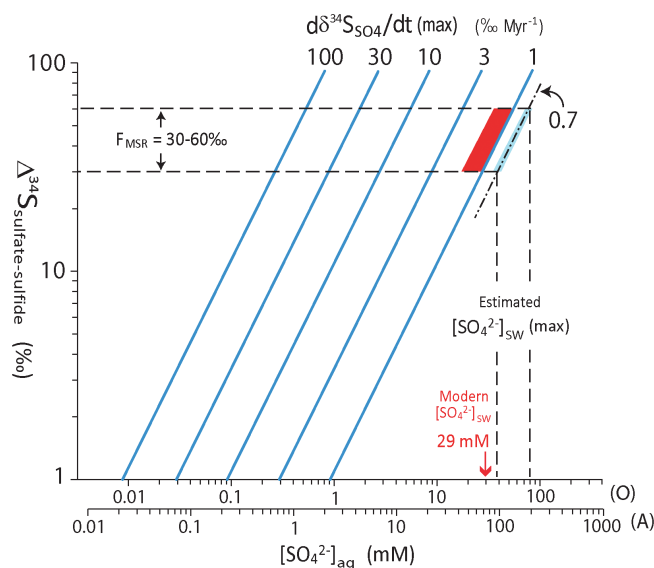


Figure 1. The rate method. On a crossplot of aqueous sulfate concentration ($[\text{SO}_4^{2-}]_{\text{aq}}$) versus S-isotopic fractionation between co-genetic sulfate and sulfide ($\Delta^{34}\text{S}_{\text{sulfate-sulfide}}$), the diagonal blue lines represent maximum rates of change in sulfate $\delta^{34}\text{S}$ (i.e., $\partial\delta^{34}\text{S}_{\text{SO}_4}/\partial t(\text{max})$). For paleomarine systems, maximum seawater sulfate concentrations ($[\text{SO}_4^{2-}]_{\text{SW}(\text{max})}$) can be estimated from the abscissa based on measured values of $\Delta^{34}\text{S}_{\text{CAS-PY}}$ and $\partial\delta^{34}\text{S}_{\text{CAS}}/\partial t(\text{max})$. The two scales on the abscissa represent $[\text{SO}_4^{2-}]_{\text{SW}}$ in oxic (O) and anoxic (A) oceans, in which pyrite burial fluxes are equal to 4×10^{13} and 10×10^{13} g yr^{-1} (i.e., 40 and 100 % of the modern total sulfur sink flux), respectively. The typical range of $\Delta^{34}\text{S}_{\text{sulfate-sulfide}}$ due to MSR fractionation in modern marine systems is 30–60 ‰ (Habicht and Canfield, 1997). The maximum rate of seawater sulfate $\delta^{34}\text{S}$ variation during the Cenozoic is ~ 0.7 ‰ Myr^{-1} (Paytan et al., 1998), yielding estimates of ~ 40 – 80 mM for $[\text{SO}_4^{2-}]_{\text{SW}}$ through projection to the abscissa (dashed lines). These estimates exceed actual modern seawater $[\text{SO}_4^{2-}]$, which is ~ 29 mM (Millero, 2005), because the *measured* maximum rate of $\partial\delta^{34}\text{S}_{\text{SO}_4}/\partial t$ (light-blue parallelogram) is less than the *theoretical* possible maximum rate (~ 1 – 2 ‰ Myr^{-1} ; red parallelogram).

to identify broad first-order trends that potentially transcend these diverse influences and that are robust over significant intervals of geologic time. Our ultimate goal is to generate useful approximations of the long-term history of sulfate in the ocean. Our results suggest that large-scale empirical relationships may exist that are not highly sensitive to influences such as organic substrate type, sulfate reduction rates, strain-specific fractionation, and other factors. We envision such local influences, as they become more completely understood, being mapped onto, and thus integrated with, the broad first-order relationships documented in this study.

2 Methods of modeling paleo-seawater sulfate concentrations

2.1 The rate method

The marine S cycle has a limited number of fluxes with fairly well-defined S-isotope ranges (Holser et al., 1989; Canfield, 2004; Bottrell and Newton, 2006), making it amenable to analysis through modeling (e.g., Halevy et al., 2012). Sub-aerial weathering yields a riverine sulfate source flux (F_Q) of $\sim 10 \times 10^{13} \text{ g yr}^{-1}$ with an average $\delta^{34}\text{S}$ of $\sim +6\text{‰}$, which is significantly lighter than the modern seawater sulfate $\delta^{34}\text{S}$ of $+20\text{‰}$. Sulfate is removed to the sediment either in an oxidized state, as carbonate-associated sulfate (CAS) or evaporite deposits, or in a reduced state, mainly as FeS or FeS₂. The oxidized sink has a flux (F_{EVAP}) of $\sim 6 \times 10^{13} \text{ g yr}^{-1}$ with a S-isotopic composition that closely mimics that of coeval seawater ($\Delta^{34}\text{S}_{\text{SW-EVAP}}$ of -4 to 0‰). The reduced sink has a flux (F_{PY}) of $\sim 4 \times 10^{13} \text{ g yr}^{-1}$ with a composition that characteristically shows a large negative fractionation relative to coeval seawater ($\Delta^{34}\text{S}_{\text{sulfate-sulfide}}$ of ~ 30 to 60‰ ; Habicht and Canfield, 1997; Canfield, 2001; Brüchert, 2004; Brunner and Bernasconi, 2005). Secular variation in seawater sulfate $\delta^{34}\text{S}$ is mainly due to changes in the relative size of the sink fluxes, with increasing (decreasing) burial of pyrite relative to sulfate leading to more (less) ^{34}S -enriched seawater sulfate (Holser et al., 1989; Bottrell and Newton, 2006; Halevy et al., 2012).

The rate method calculates a maximum seawater sulfate concentration ($[\text{SO}_4^{2-}]_{\text{SW}}(\text{max})$) based on two parameters: (1) S-isotope fractionation between cogenetic sedimentary sulfate and sulfide ($\Delta^{34}\text{S}_{\text{sulfate-sulfide}}$, as proxied by $\Delta^{34}\text{S}_{\text{CAS-PY}}$) and (2) the maximum observed rate of variation in seawater sulfate S isotopes ($\partial\delta^{34}\text{S}_{\text{SO}_4} / \partial t(\text{max})$, as proxied by $\partial\delta^{34}\text{S}_{\text{CAS}} / \partial t(\text{max})$) (Fig. 1). Rates of isotopic change for seawater sulfate are given by

$$\partial\delta^{34}\text{S}_{\text{CAS}} / \partial t = ((F_Q \times \Delta^{34}\text{S}_{\text{Q-SW}}) - (F_{\text{PY}} \times \Delta^{34}\text{S}_{\text{CAS-PY}})) / M_{\text{SW}}, \quad (1)$$

where $F_Q \times \Delta^{34}\text{S}_{\text{Q-SW}}$ is the flux-weighted difference in the isotopic compositions of the source flux and seawater (SW), $F_{\text{PY}} \times \Delta^{34}\text{S}_{\text{CAS-PY}}$ is the flux-weighted difference in the isotopic compositions of the reduced-S sink flux and seawater, and M_{SW} is the mass of seawater sulfate. The full expression represents the time-integrated influence of the source and sink fluxes on seawater sulfate $\delta^{34}\text{S}$. The maximum possible rate of change in the sulfur isotopic composition of seawater sulfate is attained when the source flux goes to zero:

$$\partial\delta^{34}\text{S}_{\text{CAS}} / \partial t(\text{max}) = F_{\text{PY}} \times \Delta^{34}\text{S}_{\text{CAS-PY}} / M_{\text{SW}}. \quad (2)$$

Reorganization of this equation allows calculation of a maximum seawater sulfate concentration from measured values

of $\Delta^{34}\text{S}_{\text{CAS-PY}}$ and $\partial\delta^{34}\text{S}_{\text{CAS}} / \partial t(\text{max})$:

$$M_{\text{SW}} = k_1 \times F_{\text{PY}} \times \Delta^{34}\text{S}_{\text{CAS-PY}} / \partial\delta^{34}\text{S}_{\text{CAS}} / \partial t(\text{max}), \quad (3)$$

$$[\text{SO}_4^{2-}]_{\text{SW}}(\text{max}) = k_2 \times M_{\text{SW}}, \quad (4)$$

where k_1 is a unit-conversion constant equal to 10^6 and k_2 is a constant relating the mass of seawater sulfate to its molar concentration that is equal to $2.22 \times 10^{-20} \text{ mM g}^{-1}$. Kah et al. (2004) assumed $F_{\text{PY}} = 10 \times 10^{13} \text{ g yr}^{-1}$, which is the total sink flux for modern seawater sulfate, in order to model $\partial\delta^{34}\text{S}_{\text{CAS}} / \partial t(\text{max})$. While this may be appropriate for intervals of widespread euxinia in the global ocean, $F_{\text{PY}} = 4 \times 10^{13} \text{ g yr}^{-1}$ (i.e., the modern sink flux) may better represent intervals with well-oxygenated oceans in which the sink fluxes of sulfate S and pyrite S are both substantial (Fig. 1). Assuming $F_{\text{PY}} = 4 \times 10^{13} \text{ g yr}^{-1}$ and values of $\Delta^{34}\text{S}_{\text{CAS-PY}}$ and $\partial\delta^{34}\text{S}_{\text{CAS}} / \partial t(\text{max})$ potentially representative of modern marine systems (e.g., 35 and 1.1‰ Myr^{-1} , respectively), Eq. 3 yields the modern seawater sulfate mass of $M_{\text{SW}} = 1.3 \times 10^{21} \text{ g}$ and Eq. (4) yields the modern seawater sulfate concentration of $\sim 29 \text{ mM}$.

Relationships among the rate-method parameters are illustrated in Fig. 1 for $\Delta^{34}\text{S}_{\text{CAS-PY}}$ from 1 to 100‰ (ordinal scale) and for discrete values of $\partial\delta^{34}\text{S}_{\text{CAS}} / \partial t(\text{max})$ ranging from 1 to 100‰ Myr^{-1} (diagonal lines). $[\text{SO}_4^{2-}]_{\text{SW}}$ increases linearly with increasing $\Delta^{34}\text{S}_{\text{CAS-PY}}$ (at constant $\partial\delta^{34}\text{S}_{\text{CAS}} / \partial t(\text{max})$) and decreases linearly with increasing $\partial\delta^{34}\text{S}_{\text{CAS}} / \partial t(\text{max})$ (at constant $\Delta^{34}\text{S}_{\text{CAS-PY}}$). The measured maximum $\partial\delta^{34}\text{S}_{\text{CAS}} / \partial t$ for a paleomarine unit is generally smaller than the theoretical maximum $\partial\delta^{34}\text{S}_{\text{SO}_4} / \partial t$ because the latter can be achieved only when the source flux of seawater sulfur is reduced (at least transiently) to zero (Kah et al., 2004), which does not routinely occur in nature. As a consequence, rate-method estimates of $[\text{SO}_4^{2-}]_{\text{SW}}$ are generally larger than actual seawater sulfate concentrations, so Eq. 4 yields the maximum likely $[\text{SO}_4^{2-}]_{\text{SW}}$ for a paleomarine unit of interest. This outcome can be illustrated by a calculation for the modern ocean, using $\Delta^{34}\text{S}_{\text{CAS-PY}}$ of ~ 30 – 60‰ and $\partial\delta^{34}\text{S}_{\text{CAS}} / \partial t(\text{max})$ of $\sim 0.7\text{‰ Myr}^{-1}$ (based on the Cenozoic seawater sulfate $\delta^{34}\text{S}$ record; Paytan et al., 1998). These inputs yield $[\text{SO}_4^{2-}]_{\text{SW}}(\text{max})$ values between ~ 40 and 80 mM , which is modestly larger than the actual modern $[\text{SO}_4^{2-}]_{\text{SW}}$ of $\sim 29 \text{ mM}$ (Fig. 1). Overestimation of modern $[\text{SO}_4^{2-}]_{\text{SW}}$ is due to measured $\partial\delta^{34}\text{S}_{\text{CAS}} / \partial t$ values for the Cenozoic ($\leq 0.7\text{‰ Myr}^{-1}$) being lower than the theoretical maximum for modern seawater (~ 1 – 2‰ Myr^{-1} ; Fig. 1). This situation is probably typical of marine units of all ages – measured rates of $\delta^{34}\text{S}_{\text{CAS}}$ variation will be lower than the theoretical maximum because the source flux of sulfur to the oceans rarely if ever goes to zero.

The results of the rate method depend on the parameterization of the pyrite burial flux (F_{PY}). This method is likely to yield an accurate estimate of seawater sulfate concentrations only if F_{PY} is inversely proportional to the residence time of sulfate in seawater (τ_{SO_4}), which basically requires the ma-

rine sulfate system to be in equilibrium. If a value for F_{PY} is chosen that is much larger or smaller than the equilibrium flux, then seawater sulfate concentrations will be overestimated or underestimated, respectively (see Appendix A1 for extended discussion). Second, the pyrite burial flux has almost certainly varied through time. Since pyrite burial flux is a component of Eqs. (2) and (3), variations in this parameter will influence calculated seawater sulfate concentrations. Phanerozoic variation in pyrite burial fluxes has been calculated in several global C–S-cycle models (e.g., Berner, 2004; Bergmann et al., 2004), although the details remain unpublished. We therefore explored the effects of variable pyrite burial fluxes on seawater sulfate estimates by using the $[\text{SO}_4^{2-}]_{\text{sw}}$ -dependent pyrite burial flux relationship of Wortmann and Chernyavsky (2007). This procedure yielded Phanerozoic $[\text{SO}_4^{2-}]_{\text{sw}}$ estimates that are close ($\pm 10\%$) to our original values (see Appendix A2 for extended discussion).

2.2 The MSR-trend method

An alternative approach to constraining ancient seawater sulfate concentrations is based on an empirical relationship to S-isotope fractionation associated with microbial sulfate reduction (F_{MSR}). We evaluated this relationship by compiling $\Delta^{34}\text{S}_{\text{sulfate-sulfide}}$ and $[\text{SO}_4^{2-}]_{\text{aq}}$ data for 81 modern depositional systems (Supplement Table S1; cf. Habicht et al., 2002). Each system was classified (1) by salinity, as freshwater (< 10 PSU), brackish (10–30 PSU), marine (30–40 PSU), or hypersaline (> 40 PSU; note that PSU stands for practical salinity units), and (2) by redox conditions, as oxic or euxinic depending on whether the chemocline was within the sediment or the water mass, respectively.

In the interests of applying uniform criteria to the generation of this data set, we followed a specific protocol. First, we adopted a modern seawater sulfate concentration of 2775 mg L^{-1} , or 28.9 mM at an average seawater density of 1025 kg m^{-3} (Millero, 2005). For brackish marine water masses, we used measured aqueous sulfate concentrations or, if unavailable, estimated dissolved sulfate concentrations from salinity data:

$$[\text{SO}_4^{2-}] = [\text{SO}_4^{2-}]_{\text{sw}} \times S/S_{\text{sw}}, \quad (5)$$

where $[\text{SO}_4^{2-}]$ and S are the sulfate concentration and salinity of the water mass of interest, respectively, and S_{sw} is the salinity of average seawater (35 PSU). Second, we used only in situ water-column measurements of aqueous sulfate $\delta^{34}\text{S}$. Third, we used sulfide $\delta^{34}\text{S}$ values either from aqueous H_2S or from sedimentary sulfide proxies located within a few centimeters of the sediment–water interface, thus avoiding sedimentary sulfides that might be significantly ^{34}S -enriched owing to sulfate-limited burial conditions (Kaplan et al., 1963; Canfield et al., 1992). However, some variation in $\delta^{34}\text{S}$ among cogenetic early-formed sedimentary sulfides is common. Acid-volatile sulfur (AVS, consisting mainly of mono-

sulfides; Rickard, 1975) tends to have a lighter sulfur isotopic composition, closer to that of the instantaneously generated H_2S at a given sediment depth, because it converts quickly to pyrite (Zaback and Pratt, 1992; Lyons, 1997). On the other hand, organic sulfur tends to be isotopically heavier owing to late-stage sulfuration of organic matter or, possibly, to fractionations associated with sulfur uptake (Zaback and Pratt, 1992; Werne et al., 2000, 2003, 2008). Although our data set includes a combination of pyrite, AVS, total reduced sulfur (TRS), and aqueous H_2S sulfur isotopic data owing to variations in sample analysis among published studies, it is weighted toward pyrite data ($n = 48$ out of a total of 81; Supplement Table S1). An analysis of $\Delta^{34}\text{S}_{\text{sulfate-sulfide}}$ variation among the multiple sulfide sources used in our study revealed no statistically significant differences (see Appendix A3). Because pyrite $\delta^{34}\text{S}$ is frequently analyzed in paleomarine studies, our MSR trend (Fig. 2) should be widely applicable to an analysis of paleo-seawater sulfate concentrations. One caveat in this regard is that $\Delta^{34}\text{S}_{\text{CAS-PY}}$ estimates for paleomarine units should be based on syngenetic or early diagenetic pyrite, as determined by well-established petrographic and geochemical criteria (e.g., Wilkin et al., 1996; Lyons and Severmann, 2006).

The protocol described above produced an internally consistent data set (Table S1) that exhibits a pronounced relationship between $\Delta^{34}\text{S}_{\text{sulfate-sulfide}}$ and $[\text{SO}_4^{2-}]_{\text{aq}}$ (Fig. 2a). Regression of $\Delta^{34}\text{S}_{\text{sulfate-sulfide}}$ on $[\text{SO}_4^{2-}]_{\text{aq}}$ yields a strong positive relationship ($r = +0.90$, $p(\alpha) < 0.01$). The trend represents an increase in $\Delta^{34}\text{S}_{\text{sulfate-sulfide}}$ from $\sim 4\text{--}6\text{‰}$ at 0.1 mM to $\sim 30\text{--}60\text{‰}$ at 29 mM (i.e., modern seawater $[\text{SO}_4^{2-}]$). $\Delta^{34}\text{S}_{\text{sulfate-sulfide}}$ appears to peak at $[\text{SO}_4^{2-}]_{\text{aq}}$ of 15–20 mM, with a mean value $\sim 5\text{--}10\text{‰}$ greater than for $[\text{SO}_4^{2-}]_{\text{aq}}$ of 29 mM, but this effect is small relative to the overall relationship between $\Delta^{34}\text{S}_{\text{sulfate-sulfide}}$ and $[\text{SO}_4^{2-}]_{\text{aq}}$, and we did not factor it separately into the regression analysis. For hypersaline environments in which $[\text{SO}_4^{2-}]_{\text{aq}} > 29 \text{ mM}$, $\Delta^{34}\text{S}_{\text{sulfate-sulfide}}$ does not continue to rise but, rather, shows roughly the same range as for modern seawater (Fig. 2a). Finally, we analyzed the data by redox environment and found only minor and statistically insignificant differences between oxic and euxinic settings (note that hypersaline environments were not included in this analysis). The distributions of the oxic and euxinic data sets show broad overlap (Fig. 2a), so benthic redox conditions appear to exhibit no discernible influence on the relationship of $\Delta^{34}\text{S}_{\text{sulfate-sulfide}}$ to $[\text{SO}_4^{2-}]_{\text{aq}}$.

Our analysis demonstrates that a strong relationship exists between F_{MSR} and $[\text{SO}_4^{2-}]_{\text{aq}}$ in natural aqueous systems ($r = +0.90$, $p(\alpha) < 0.01$; Fig. 2a). Our results are similar to, although more linear and more statistically robust than, those reported by Habicht et al. (2002) on the basis of culture experiments. We recognize that there are multiple environmental and physiological controls on fractionation by sulfate reducers (see Sect. 3), and that under certain natural and ex-

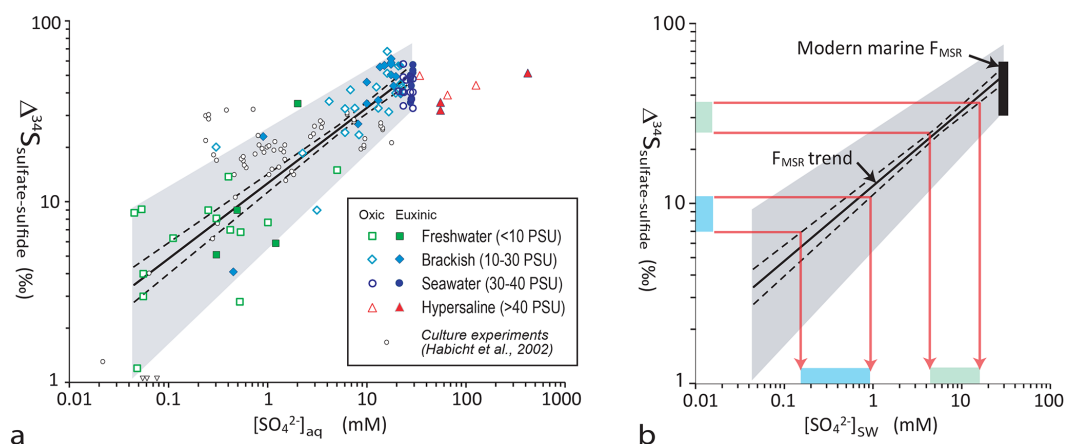


Figure 2. The MSR-trend method. **(a)** Data from 81 modern aqueous systems (Table S1). The non-hypersaline environments ($n = 75$) yield a linear regression (solid line; $y = 0.42x + 1.10$ in log units) with $r = +0.90$ t statistic = 1.99, ($p(\alpha) < 0.01$) and a limited uncertainty range (dashed lines). The MSR trend thus represents a process with an order of reaction (n) of 0.42 and a rate constant (k) of 1.10 (cf. Jones et al., 2007). The gray field encloses most of the data from Table S1 and highlights the overall trend. Analysis of the data set by redox environment yielded statistically indistinguishable trends for oxic ($y = 0.48x + 1.10$; $r = +0.88$, $n = 44$, $p(\alpha) < 0.01$) and euxinic settings ($y = 0.40x + 1.06$; $r = +0.89$, $n = 31$, $p(\alpha) < 0.01$). The Habicht et al. (2002) data set of 60 sulfate-reducing microbial (SRM) culture values is shown for comparison; these data have been converted to log–log format, and data points that are off-scale (i.e., $\Delta^{34}\text{S}_{\text{sulfate-sulfide}} < 1\%$) are shown by triangles on the abscissa. Neither the six hypersaline environments in our data set (red symbols) nor the Habicht et al. data (small open circles) were included in the regression analysis. **(b)** Use of the MSR trend to estimate paleo-seawater $[\text{SO}_4^{2-}]_{\text{aq}}$. Measured values of $\Delta^{34}\text{S}_{\text{sulfate-sulfide}}$ are projected from the ordinal scale to the MSR trend and then to the abscissa. Note that uncertainty in the slope of the MSR trend is accommodated by projection to the upper uncertainty limit for $\Delta^{34}\text{S}_{\text{sulfate-sulfide}}$ maxima and to the lower uncertainty limit for $\Delta^{34}\text{S}_{\text{sulfate-sulfide}}$ minima. The vertical black bar at $[\text{SO}_4^{2-}]_{\text{aq}} = 1.45$ (i.e., the modern seawater sulfate concentration of 29 mM) represents the range of F_{MSR} variation among modern marine SRM communities.

perimental conditions the relationship of F_{MSR} to $[\text{SO}_4^{2-}]_{\text{aq}}$ can deviate markedly from that in our data set. However, the pattern of covariation between F_{MSR} and $[\text{SO}_4^{2-}]_{\text{aq}}$ documented here represents a robust relationship that appears to hold for a wide range of natural environments, reflecting the possibly near-ubiquitous influence of $[\text{SO}_4^{2-}]_{\text{aq}}$ on F_{MSR} . The apparent breakdown of this relationship in hypersaline environments (Fig. 2a) needs further testing; our data set for hypersaline environments is too small ($n = 6$) to reach firm conclusions. However, the strength of the $F_{\text{MSR}}-[\text{SO}_4^{2-}]_{\text{aq}}$ relationship for water masses with salinities ranging up to ~ 40 PSU suggests that it can serve as a basis for evaluating the $[\text{SO}_4^{2-}]_{\text{aq}}$ of ancient seawater. Seawater $[\text{SO}_4^{2-}]$ can be estimated graphically by projecting measured values of $\Delta^{34}\text{S}_{\text{CAS-PY}}$ from the ordinal scale to the MSR trend and then to the abscissa (Fig. 2b), or by using the following empirical equation:

$$\log[\text{SO}_4^{2-}] = \left(\log(\Delta^{34}\text{S}_{\text{CAS-PY}}) - 1.10 \right) / 0.42. \quad (6)$$

The upper and lower uncertainty limits for estimates of seawater $[\text{SO}_4^{2-}]$ based on this relationship are

$$\log[\text{SO}_4^{2-}] = \left(\log(\Delta^{34}\text{S}_{\text{CAS-PY}}) - 1.18 \right) / 0.40 \text{ (upper limit)}, \quad (7)$$

$$\log[\text{SO}_4^{2-}] = \left(\log(\Delta^{34}\text{S}_{\text{CAS-PY}}) - 1.02 \right) / 0.44 \text{ (lower limit)}. \quad (8)$$

In order to account for uncertainties in $\Delta^{34}\text{S}_{\text{CAS-PY}}$ as well as the F_{MSR} regression, estimates of minimum $[\text{SO}_4^{2-}]_{\text{SW}}$ should make use of minimum $\Delta^{34}\text{S}_{\text{CAS-PY}}$ values in combination with the upper uncertainty limit equation (Eq. 7), and estimates of maximum $[\text{SO}_4^{2-}]_{\text{SW}}$ should make use of maximum $\Delta^{34}\text{S}_{\text{CAS-PY}}$ values in combination with the lower uncertainty limit equation (Eq. 8; Fig. 2b).

3 Controls on fractionation by microbial sulfate reducers

The biogeochemical nature of the MSR process and its associated S-isotope fractionations have been extensively investigated in earlier studies. Sulfate reducers preferentially utilize sulfate containing ^{32}S during dissimilatory reduction to hydrogen sulfide in conjunction with the anaerobic decay

of organic matter (Kaplan, 1983; Canfield, 2001; Bradley et al., 2011). The exact controls on this isotopic discrimination continue to be a topic of intense debate. The paradigmatic view is that this fractionation is mainly a kinetic effect associated with the rate-limiting step for intracellular sulfate processing, although it is known that fractionation also may accompany sulfate transport across the cell membrane (Rees, 1973; Detmers et al., 2001; Brüchert, 2004; Bradley et al., 2011). The kinetic effect is thought to be dependent on aqueous sulfate concentrations, with substantially larger fractionations associated with $[\text{SO}_4^{2-}]_{\text{aq}} > \sim 200 \mu\text{M}$ (Habicht et al., 2002; Gomes and Hurtgen, 2013; but see Canfield, 2001, for a counter example). Rees (1973) proposed a maximum discrimination of 46‰, but the theoretical basis for this value was reassessed by Brunner and Bernasconi (2005). Recent studies have documented F_{MSR} as large as 66‰ in culture experiments (Sim et al., 2011a) and 70–80‰ in natural systems (Rudnicki et al., 2001; Wortmann et al., 2001; Canfield et al., 2010). Even larger fractionations have been reported, but these are generally considered to be the result of multi-stage disproportionation of intermediate-oxidation-state sulfur compounds (Canfield and Thamdrup, 1994).

Investigations of natural and experimental systems have documented a number of additional controls on F_{MSR} . One of the most important controls is f_{SO_4} , i.e., the fraction of remaining dissolved sulfate (Gomes and Hurtgen, 2013). In “open systems” containing a high concentration of dissolved sulfate (e.g., the modern ocean), f_{SO_4} does not vary measurably from 1.0 because the quantity of sulfate converted to sulfide via MSR is a small fraction of the total aqueous sulfate inventory. In this case, the produced sulfide will show the maximum degree of fractionation, which is typically ~ 30 to 60 ‰ in modern marine systems (Fig. 2a; Table S1). In contrast, in “closed systems” in which the aqueous sulfate inventory is limited (e.g., sediment porewaters or low-sulfate freshwater systems), dissolved sulfate concentrations can be substantially reduced or completely depleted through MSR, causing f_{SO_4} to evolve toward zero. As $[\text{SO}_4^{2-}]_{\text{aq}}$ becomes smaller, sulfate reducers utilize a progressively larger fraction of the total dissolved sulfate pool, reducing the effective fractionation to small values (Habicht et al., 2002; Gomes and Hurtgen, 2013). In these settings, the aggregate $\delta^{34}\text{S}$ composition of the produced sulfide approaches that of the original aqueous sulfate inventory, and $\Delta^{34}\text{S}_{\text{sulfate-sulfide}}$ approaches zero (Kaplan, 1983; Habicht et al., 2002). In a macro sense, f_{SO_4} can be proxied by $[\text{SO}_4^{2-}]_{\text{aq}}$, accounting for the strong first-order relationship between the latter parameter and $\Delta^{34}\text{S}_{\text{sulfate-sulfide}}$ ($r = +0.90$, $p(\alpha) < 0.01$; Fig. 2a). However, not all researchers agree on the importance of f_{SO_4} as a control on F_{MSR} (e.g., Leavitt et al., 2013).

Other factors may influence F_{MSR} under certain conditions. First, different dissimilatory reduction pathways yield different isotopic discriminations. Oxidation of organic substrates to CO_2 yields larger fractionations (~ 30 – 60 ‰) than oxidation to acetate (< 18 ‰) (Detmers et al., 2001; Brüchert

et al., 2001; Brüchert, 2004). Incomplete oxidation of organic substrates is a feature characteristic of sulfate reducers in hypersaline environments (Habicht and Canfield, 1997; Oren, 1999; Detmers et al., 2001; Stam et al., 2010) and may account for the somewhat smaller fractionations typically encountered in such environments (Fig. 2a). Second, the type of organic substrate also matters, as ethanol, lactate, glucose, and other compounds yield different fractionations under otherwise similar conditions (Canfield, 2001; Detmers et al., 2001; Kleikemper et al., 2004; Sim et al., 2011b). Third, sulfate reduction rates may also influence F_{MSR} , with higher rates associated with smaller isotopic discriminations (Kaplan and Rittenberg, 1964; Kemp and Thode, 1968; Rees, 1973; Chambers et al., 1975; Habicht and Canfield, 1996; Brüchert et al., 2001; Canfield, 2001; Brunner and Bernasconi, 2005). Recent experiments by Leavitt et al. (2013) showed that F_{MSR} declines rapidly with increasing sulfate reduction rates before leveling off at ~ 15 – 20 ‰ at rates $> 50 \text{ mmol H}_2\text{S per unit substrate per day}$. Habicht and Canfield (2001) hypothesized that F_{MSR} is only incidentally related to sulfate reduction rates because both are correlated with the disproportionation of intermediate-oxidation-state S compounds by sulfur-oxidizing bacteria, which have probably been present since the Archean (Johnston et al., 2005; Wacey et al., 2010). Fourth, cell external sulfide (CES) concentrations, when high, can cause back-diffusion of sulfide into cells, with subsequent oxidative recycling to sulfate (Brunner and Bernasconi, 2005; Eckert et al., 2011). Finally, temperature has been shown to affect F_{MSR} in some studies (e.g., Canfield et al., 2006) but not others (e.g., Detmers et al., 2001). The influence of temperature on F_{MSR} may operate through the species-specific temperature dependence of enzymes.

Research to date clearly shows that controls on microbial sulfate reduction are complex and incompletely understood. This situation reflects the diverse composition of the microbial communities that process sulfur in the marine environment and the range of isotopic fractionations associated with those processes (Brüchert, 2004). Yet even though multiple environmental and physiological factors influence F_{MSR} , the strength of its relationship to $[\text{SO}_4^{2-}]_{\text{aq}}$, as documented in this study (Fig. 2a), implies that aqueous sulfate concentrations are the dominant first-order control on F_{MSR} , and that other factors such as organic substrate, rates of MSR, and temperature are second-order controls whose effects may be randomized at a larger scale and do not obscure the dominant influence of $[\text{SO}_4^{2-}]_{\text{aq}}$ in most environments. Whether the quantitative form of our $F_{\text{MSR}}-[\text{SO}_4^{2-}]_{\text{aq}}$ relationship is unique to the present or valid for the geologic past is unclear. Microbial S-cycling processes are thought to have been conservative through time (e.g., Wacey et al., 2010), although lower atmospheric $p\text{O}_2$ prior to $\sim 635 \text{ Ma}$ may have limited disproportionation of intermediate-oxidation-state sulfur compounds and thus the potential for large fractionations

(Habicht and Canfield, 2001; Sørensen and Canfield, 2004; Johnston et al., 2005). In the following analysis, we adopt the $F_{\text{MSR}}\text{--}[\text{SO}_4^{2-}]_{\text{aq}}$ relationship of Fig. 2a as a basis for evaluating the $[\text{SO}_4^{2-}]_{\text{aq}}$ of ancient seawater from 635 Ma to the present.

4 Estimation of seawater sulfate concentrations since 635 Ma

4.1 General considerations and modeling protocol

The rate and MSR-trend methods can be applied to analysis of long-term variation in seawater sulfate concentrations. Although both methods utilize measured values of $\Delta^{34}\text{S}_{\text{sulfate-sulfide}}$ as a proxy for F_{MSR} , they are quasi-independent in having different transform functions. The transform function of the rate method (Eqs. 3 and 4) makes use of observed rates of seawater sulfate S-isotopic variation (i.e., $\partial\delta^{34}\text{S}_{\text{CAS}}/\partial t(\text{max})$), whereas that of the MSR-trend method (Eqs. 6–8) makes use of an empirical relationship between F_{MSR} and $[\text{SO}_4^{2-}]_{\text{aq}}$. The two methods are applicable over approximately the same range of $[\text{SO}_4^{2-}]_{\text{sw}}$ concentrations ($\sim 0.1\text{--}30\text{ mM}$). However, their transform functions have different sensitivities to $[\text{SO}_4^{2-}]_{\text{sw}}$, with that of the MSR-trend method being greater as reflected in its lower slope ($m = 0.42$; Fig. 2) compared with that of the rate method ($m = 1.0$; Fig. 1). Thus, a combination of the two methods may be the most useful approach to constraining ancient seawater $[\text{SO}_4^{2-}]$. Because the rate method yields estimates of maximum likely $[\text{SO}_4^{2-}]_{\text{sw}}$, it should generally yield a higher estimated sulfate concentration than the MSR-trend method, which estimates the mean $[\text{SO}_4^{2-}]_{\text{sw}}$ of the time interval of interest. The pairing of these procedures is thus useful in providing both mean and maximum estimates of paleo-seawater sulfate concentrations. Combining these two methods is also useful in providing a check on the robustness of the results. For example, if the maximum estimate yielded by the rate method is less than the mean estimate yielded by the MSR-trend method, then the results should be considered unreliable.

Both the rate and MSR-trend methods require defined input variables for calculation of paleo-seawater $[\text{SO}_4^{2-}]$. For the rate method, a record of secular variation in seawater sulfate $\delta^{34}\text{S}$ is needed from which to calculate $\partial\delta^{34}\text{S}_{\text{CAS}}/\partial t$. We generated a seawater sulfate $\delta^{34}\text{S}$ record for the Phanerozoic by combining published $\delta^{34}\text{S}_{\text{CAS}}$ data sets for the Cenozoic (Paytan et al., 1998), Cretaceous (Paytan et al., 2004), and pre-Cretaceous (Kampschulte and Strauss, 2004) (Table S2; Fig. 3a). We calculated locally weighted scatterplot smoothing (LOWESS) curves for this composite record as per the methodology of Song et al. (2014). LOWESS curves were generated at both a low frequency (i.e., 5 Myr steps) and a high frequency (i.e., 1 Myr steps), the latter resulting in less smoothing of the long-term $\delta^{34}\text{S}_{\text{CAS}}$ trend (Fig. 3a). The

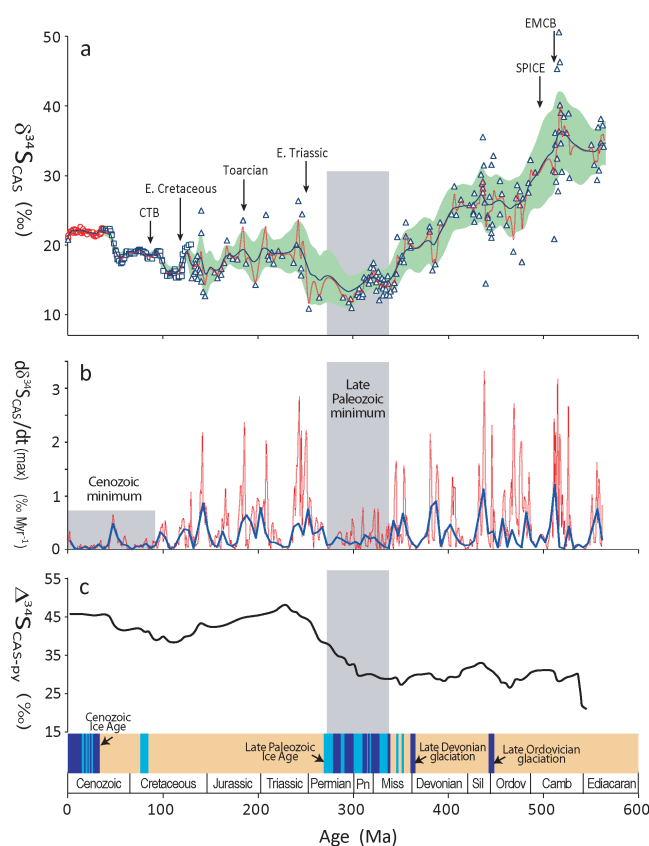


Figure 3. (a) Phanerozoic seawater sulfate $\delta^{34}\text{S}$. Data sources: Cenozoic (Paytan et al., 1998; red circles), Cretaceous (Paytan et al., 2004; black squares), and pre-Cretaceous (Kampschulte and Strauss, 2004; blue triangles; Table S2). Secular variation in $\delta^{34}\text{S}_{\text{SO}_4\text{--sw}}$ is shown by a mean LOWESS curve (blue line for low-resolution (5 Myr) and red line for high-resolution (1 Myr) records) and a standard deviation ($\pm 1\sigma$) range (green field for low-resolution record; Table S3). Pre-Cretaceous and Cretaceous–Cenozoic estimates of $\delta^{34}\text{S}_{\text{SO}_4\text{--sw}}$ have uncertainties of $\pm 2\text{--}7\text{‰}$ and $\pm < 1\text{‰}$, respectively. The labels represent four short-term ($< 2\text{ Myr}$) intervals of high-frequency $\partial\delta^{34}\text{S}_{\text{SO}_4}/\partial t$ variation (EMCB: early–middle Cambrian boundary; SPICE: Steptoean positive carbon isotope excursion; CTB: Cenomanian–Turonian boundary). (b) Rate of seawater $\delta^{34}\text{S}$ variation ($\partial\delta^{34}\text{S}_{\text{SO}_4}/\partial t$) as calculated from the seawater sulfate $\delta^{34}\text{S}$ LOWESS curves. The maximum Phanerozoic $\partial\delta^{34}\text{S}_{\text{SO}_4}/\partial t$ is $< 4\text{‰ Myr}^{-1}$, although rates of 10 to $> 50\text{‰ Myr}^{-1}$ have been reported from some high-resolution CAS studies. (c) $\Delta^{34}\text{S}_{\text{CAS-PY}}$ for Phanerozoic marine sediments (data from Fig. 3 of Wu et al., 2010). The continental glaciation record is adapted from Montañez et al. (2011); all ages were converted to the Gradstein et al. (2012) timescale.

LOWESS curves were then used to calculate rates of change in seawater sulfate concentrations ($\partial\delta^{34}\text{S}_{\text{SO}_4}/\partial t$) through the Phanerozoic (Fig. 3b). For both the rate and MSR-trend methods, $\Delta^{34}\text{S}_{\text{sulfate-sulfide}}$ is a defined input variable. As a proxy, we utilized the Phanerozoic $\Delta^{34}\text{S}_{\text{CAS-PY}}$ record of Wu et al. (2010). According to this record, $\Delta^{34}\text{S}_{\text{CAS-PY}}$ averaged

$30 \pm 3 \text{ ‰}$ from 540 to 300 Ma, increased gradually from 30 to 45 ‰ between 300 and 270 Ma, and then fluctuated around $42 \pm 5 \text{ ‰}$ from 270 to 0 Ma (Fig. 3c).

4.2 Long-term variation in seawater sulfate concentrations

Our composite record shows that seawater sulfate $\delta^{34}\text{S}$ was heavy ($\sim 30\text{--}40 \text{ ‰}$) during the Ediacaran to middle Cambrian, declined steeply during the late Cambrian to Early Ordovician, and stabilized at intermediate values ($\sim 20\text{--}30 \text{ ‰}$) during the Middle Ordovician to Early Devonian (Table S3; Fig. 3a). Sulfate $\delta^{34}\text{S}$ declined further during the Middle Devonian to Early Mississippian, reaching a minimum of $\sim 12\text{--}16 \text{ ‰}$ during the mid-Mississippian to the end of the Permian. Sulfate $\delta^{34}\text{S}$ then rose sharply to $\sim 20 \text{ ‰}$ during the Early Triassic, before declining slightly to a local minimum of $\sim 15 \text{ ‰}$ around the Jurassic–Cretaceous boundary. Sulfate $\delta^{34}\text{S}$ rose slowly during the Cretaceous and early Cenozoic, increased rapidly from 17 to 22 ‰ at 40–50 Ma, and then stabilized at 21–23 ‰ during the mid- to late Cenozoic (Fig. 3a). The low-frequency LOWESS curve exhibits low rates of $\delta^{34}\text{S}$ variation, with a mean of $0.25(\pm 0.17) \text{ ‰ Myr}^{-1}$ and a maximum of $\sim 0.8 \text{ ‰ Myr}^{-1}$ (Fig. 3b). The high-frequency LOWESS curve exhibits somewhat higher rates of $\delta^{34}\text{S}$ variation, with a mean of $0.40(\pm 0.45) \text{ ‰ Myr}^{-1}$ and a maximum of $\sim 2.5 \text{ ‰ Myr}^{-1}$ (Fig. 3b). Both curves show exceptionally low rates of seawater sulfate $\delta^{34}\text{S}$ variation during the Late Cretaceous and Cenozoic (the “Cenozoic minimum”) and the mid-Mississippian to mid-Permian (the “Late Paleozoic minimum”).

Our reconstructions of mean and maximum seawater sulfate concentrations through the Phanerozoic, based respectively on the MSR-trend and rate methods, are shown in Fig. 4. The mean curve suggests that $[\text{SO}_4^{2-}]_{\text{SW}}$ was low in the late Ediacaran ($\sim 1\text{--}4 \text{ mM}$) but rose sharply in the early Cambrian (to $\sim 3\text{--}15 \text{ mM}$) and remained in that range until the Permian. A long, slow rise in $[\text{SO}_4^{2-}]_{\text{SW}}$ began in the Early Permian and culminated at $\sim 12\text{--}38 \text{ mM}$ in the Middle Triassic. Subsequently, $[\text{SO}_4^{2-}]_{\text{SW}}$ declined slightly by the mid-Cretaceous (to $\sim 7\text{--}25 \text{ mM}$) and then rose slightly during the Late Cretaceous to early Cenozoic (to 11–35 mM). The standard deviation range for the mean curve (blue band) suggests an uncertainty of plus or minus a factor of $\sim 2x$ in the mean estimate, with the magnitude of the uncertainty shrinking modestly from the Cambrian to the present. The modern seawater sulfate concentration of 29 mM falls within the standard deviation range of the mean trend (Fig. 4).

A maximum $[\text{SO}_4^{2-}]_{\text{SW}}$ curve can be calculated for both the low- and high-frequency Phanerozoic $\delta^{34}\text{S}$ records of Fig. 3a. The low- and high-frequency maximum $[\text{SO}_4^{2-}]_{\text{SW}}$ curves (shown as black and red lines, respectively, in Fig. 4) mirror the upward trend through the Phanerozoic seen in the mean curve and thus are consistent with a factor of $\sim 4x$ increase in seawater sulfate concentrations since the early

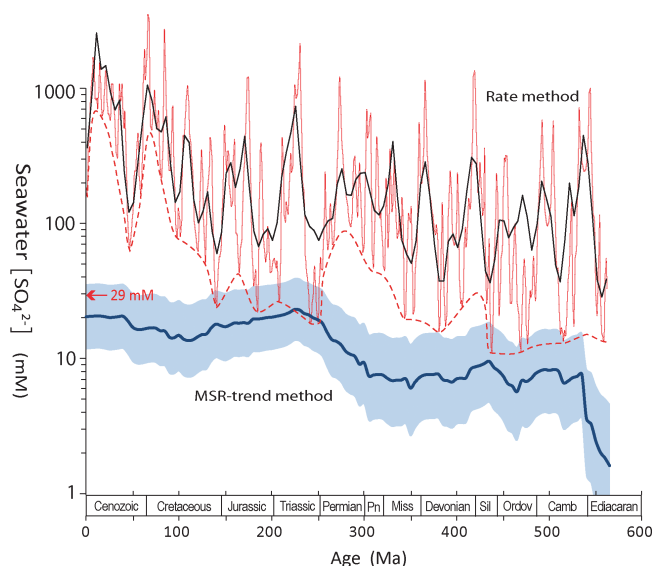


Figure 4. Phanerozoic seawater $[\text{SO}_4^{2-}]$ (Table S3). The MSR-trend method (Eqs. 6–8) yields an estimate of mean $[\text{SO}_4^{2-}]_{\text{SW}}$ (blue curve; bracketed by a $\pm 1\sigma$ band). The rate method (Eqs. 3 and 4) yields the maximum possible $[\text{SO}_4^{2-}]_{\text{SW}}$; the black and red curves show maximum values based on the low- and high-frequency Phanerozoic $\delta^{34}\text{S}_{\text{CAS}}$ records, respectively (Fig. 3a), and the dashed red line represents the lower envelope of the high-frequency curve. The modern seawater $[\text{SO}_4^{2-}]$ of $\sim 29 \text{ mM}$ is shown by the red arrow.

Cambrian. Although the maximum $[\text{SO}_4^{2-}]_{\text{SW}}$ curves exhibit values that are mostly unrealistically large, it is worth noting that (1) these curves represent the maximum possible, not the most likely, concentrations of seawater sulfate and that (2) the smallest values on the maximum curves are more robust constraints on $[\text{SO}_4^{2-}]_{\text{SW}}$ than the largest values. The second observation is based on the fact that the smallest values derive from the largest measured rates of $\delta^{34}\text{S}_{\text{CAS}}$ variation (Fig. 3b), i.e., those rates that most closely approach the theoretical maximum, whereas the largest values are associated with intervals of little or no $\delta^{34}\text{S}_{\text{CAS}}$ variation. Thus, the lower envelope of maximum $[\text{SO}_4^{2-}]_{\text{SW}}$ values (dashed line, Fig. 4) provides a more useful constraint on seawater sulfate concentrations than the full curve. We also suggest that, although the upper limits on $[\text{SO}_4^{2-}]_{\text{SW}}$ imposed by the rate method may have limited utility for assessment of Phanerozoic seawater sulfate, this method may be of greater value in analyzing Archean and Proterozoic seawater sulfate concentrations, which are thought to have been quite low ($< 1 \text{ mM}$; Kah et al., 2004; Canfield et al., 2007; Planavsky et al., 2012).

The results of the rate method are dependent on several factors that influence the estimation of rates of seawater sulfate $\delta^{34}\text{S}$ variation. $\partial\delta^{34}\text{S}_{\text{SO}_4} / \partial t(\text{max})$ may be overestimated if there is an increase in $\delta^{34}\text{S}_{\text{CAS}}$ variance due to diagenesis or procedural artifacts during CAS extrac-

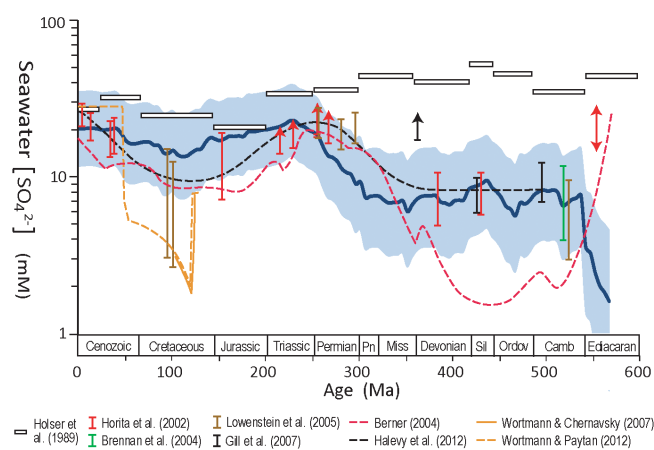


Figure 5. Comparison of Phanerozoic seawater sulfate $[\text{SO}_4^{2-}]$ records. The mean trend of the present study is shown by a thick blue line, with the $\pm 1\sigma$ uncertainty range shown as a blue band. Estimates are based either on fluid-inclusion studies (Horita et al., 2002; Brennan et al., 2004; Lowenstein et al., 2005) or C–S-cycle modeling (Holser et al., 1989; Berner, 2004; Gill et al., 2007; Wortmann and Chernavsky, 2007; Wortmann and Paytan, 2012; Halevy et al., 2012). Arrows indicate unconstrained minimum or maximum values.

tion, or it may be underestimated if there is a decrease in $\delta^{34}\text{S}_{\text{CAS}}$ variance due to diagenesis or procedural data smoothing. Data smoothing is inherent in the calculation of LOWESS curves (cf. Song et al., 2014), and underestimation of $\partial\delta^{34}\text{S}_{\text{SO}_4}/\partial t(\text{max})$ is thus almost certain when smoothed $\delta^{34}\text{S}_{\text{SO}_4}$ data sets are used as inputs. It may be responsible for the absence of short-term excursions in our Phanerozoic $[\text{SO}_4^{2-}]_{\text{SW}}$ curve (Fig. 3a), since a number of short (< 2 Myr) intervals of strongly elevated $\partial\delta^{34}\text{S}_{\text{SO}_4}/\partial t$ rates have been documented for the Phanerozoic (Wortmann and Chernavsky, 2007; Adams et al., 2010; Gill et al., 2011a,b; Newton et al., 2011; Wotte et al., 2012; Owens et al., 2013; Song et al., 2014; see Sect. 4.3). During these intervals, $\partial\delta^{34}\text{S}_{\text{SO}_4}/\partial t$ ranged from 10 to > 50 ‰ Myr $^{-1}$ (Table S4), rates that are considerably higher than peak rates for the long-term $\delta^{34}\text{S}_{\text{CAS}}$ curve (ca. 2–4 ‰ Myr $^{-1}$; Fig. 3b). Because lower values for $\partial\delta^{34}\text{S}_{\text{SO}_4}/\partial t(\text{max})$ yield higher maximum estimates of $[\text{SO}_4^{2-}]$ for ancient seawater (Eqs. 3 and 4), smoothing may account for some of the divergence between the mean and maximum trends in Fig. 4. The existence of such short-term episodes of seawater sulfate drawdown during the Phanerozoic has been attributed to several causes, including episodic massive evaporite deposition (Wortmann and Paytan, 2012) and reduced ventilation of marine sediments and a consequent increase in MSR in the aftermath of mass extinction events (Canfield and Farquhar, 2009).

Comparison of our Phanerozoic seawater sulfate concentration curve with previously published estimates reveals similarities and differences (Fig. 5). Most of these records exhibit a local minimum during the Jurassic or Cretaceous,

although the absolute estimates of $[\text{SO}_4^{2-}]$ for this minimum vary widely (~ 2 to 25 mM). Our higher estimates (~ 13 –16 mM) compared to those of Wortmann and Paytan (2012) (uniformly < 7 mM) may be a consequence of our choice of input data set, i.e., the Phanerozoic $\Delta^{34}\text{S}_{\text{CAS-PY}}$ record of Wu et al. (2010). The latter is based on a large compilative data set that yielded a strongly time-averaged trend, which is likely to have dampened variation in our $[\text{SO}_4^{2-}]_{\text{SW}}$ estimates. The various records are also in agreement that seawater sulfate was elevated during the Permian–Triassic, with concentrations of ~ 15 –30 mM. The records diverge prior to the Permian, however, with one model (Holser et al., 1989) suggesting high values (30–50 mM) and another model (Berner, 2004) low values (< 2 mM) through the mid-Paleozoic. Our model indicates intermediate sulfate concentrations (5–10 mM) at that time (Fig. 5). The various records also show dissimilar patterns across the Ediacaran–Cambrian boundary, with uniformly high values in the Holser et al. (1989) model and steeply falling values in the Berner (2004) model. The results of the present study favor a steep rise in seawater sulfate at this boundary. Our Phanerozoic seawater sulfate concentration record, along with that of Halevy et al. (2012), is in good agreement with the available fluid-inclusion data (Fig. 5) and thus appears generally robust, although it probably does not capture short-term episodes of seawater sulfate drawdown (see Sect. 4.3).

Our reconstruction of long-term secular variation in seawater sulfate concentrations shows a strong relationship to first-order Phanerozoic climate cycles (cf. Algeo et al., 2014). In particular, the interval of the Late Paleozoic Ice Age, which lasted from the mid-Mississippian through the mid-Permian, was characterized by a major change in the oceanic sulfate reservoir. At that time, minimum values developed for both seawater sulfate $\delta^{34}\text{S}$ (~ 12 –16 ‰; Fig. 3a) and rates of $\delta^{34}\text{S}_{\text{SO}_4}$ variation (< 1 ‰ Myr $^{-1}$; Fig. 3b), accompanied by a concurrent increase in sulfate–sulfide fractionation (from < 30 to > 40 ‰; Fig. 3c). Whether these are general features of seawater sulfate during icehouse climate modes is not entirely certain. A second interval of global climatic cooling and continental glaciation during the Late Cretaceous and Cenozoic also shows low rates of $\delta^{34}\text{S}_{\text{SO}_4}$ variation and an increase in sulfate–sulfide fractionation but, in contrast to the Late Paleozoic, ^{34}S -enriched and relatively stable seawater sulfate $\delta^{34}\text{S}$ values (Fig. 3). The greater stability of seawater sulfate $\delta^{34}\text{S}$ during the Cenozoic relative to the Late Paleozoic may be due to a long-term increase in total seawater sulfate mass (Figs. 4–5). We hypothesize that the Late Paleozoic was characterized by low rates of pyrite burial (hence, lower $\delta^{34}\text{S}_{\text{SO}_4}$) and a consequent increase in the mass of seawater sulfate (hence, lower $\partial\delta^{34}\text{S}_{\text{SO}_4}/\partial t$) (cf. Halevy et al., 2012). Low rates of pyrite burial at that time may have been due to a combination of lower sea-level elevations (reducing the total shelf area available for sulfate reduction; cf. Halevy et al., 2012; Algeo et al., 2014), enhanced oceanic

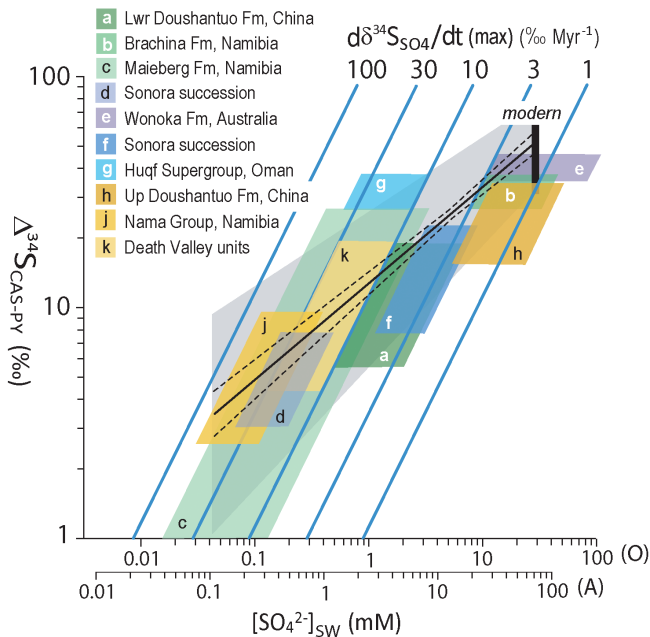


Figure 6. Analysis of seawater sulfate concentrations for 10 late Neoproterozoic marine units. The parallelogram for each unit was generated using the rate method. A summary of results and data sources is given in Table S4; other details as in Figs. 1–2.

ventilation (increasing aerobic decay of organic matter), and increased burial of organic matter in low-sulfate freshwater settings, which was linked to the spread of terrestrial floras (DiMichele and Hook, 1992).

4.3 High-frequency variation in seawater sulfate during the Neoproterozoic and Phanerozoic

We applied the rate and MSR-trend methods to an analysis of short-term variation in $[\text{SO}_4^{2-}]_{\text{SW}}$ during selected intervals of the Neoproterozoic and Phanerozoic for which high-resolution $\delta^{34}\text{S}_{\text{CAS}}$ studies are available. For the Neoproterozoic, recent studies have provided S-isotope records from a number of sites globally as well as improved radiometric geochronologic constraints that are needed for the rate method. Based on these studies, we have estimated $\partial\delta^{34}\text{S}_{\text{SO}_4}/\partial t(\text{max})$ for 10 late Neoproterozoic units (Table S4; Fig. 6). Radiometric studies of the Doushantuo Formation in South China (Halverson et al., 2005; Zhang et al., 2005, 2008) provided key ages from which we calculated $\partial\delta^{34}\text{S}_{\text{CAS}}/\partial t(\text{max})$ of 5‰ Myr^{-1} at $\sim 636\text{--}633\text{ Ma}$ and 1.3‰ Myr^{-1} at $\sim 568\text{--}551\text{ Ma}$ (McFadden et al., 2008; Li et al., 2010). The Neoproterozoic succession of Sonora, Mexico, yielded $\partial\delta^{34}\text{S}_{\text{CAS}}/\partial t(\text{max})$ estimates of 6 and 4‰ Myr^{-1} (Lloyd et al., 2012, 2013). The latest Neoproterozoic Zarl's Formation (Nama Group) in Namibia and upper Huqf Supergroup in Oman yielded $\partial\delta^{34}\text{S}_{\text{CAS}}/\partial t(\text{max})$ estimates of 20‰ Myr^{-1} and 40‰ Myr^{-1} , respectively, at 549–

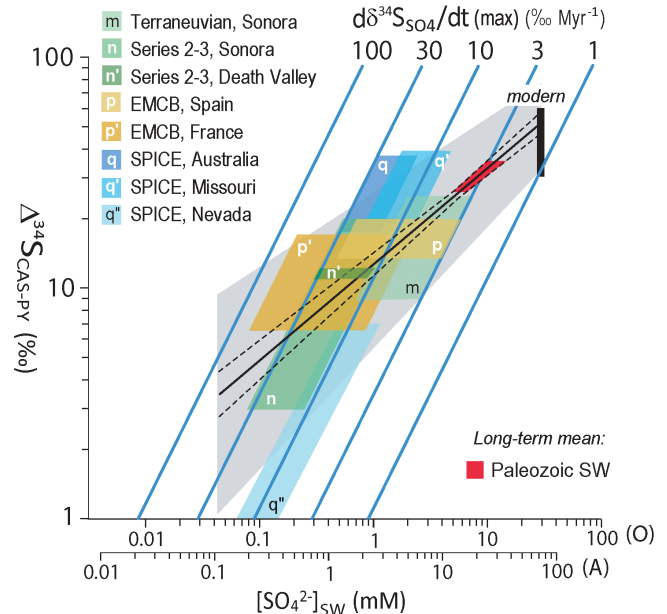


Figure 7. Analysis of seawater sulfate concentrations for eight Paleozoic marine units. The parallelogram for each unit was generated using the rate method. The red field represents the long-term average $\Delta^{34}\text{S}_{\text{CAS-PY}}$ for the Paleozoic based on data in Wu et al. (2010). A summary of results and data sources is given in Table S4; other details as in Figs. 1–2.

547 Ma (Fike and Grotzinger, 2008; Ries et al., 2009). The rate method yielded $[\text{SO}_4^{2-}]_{\text{SW}}$ estimates ranging from < 0.1 to $> 100\text{ mM}$, with most between ~ 1 and 10 mM (Table S4). The MSR-trend method yielded $[\text{SO}_4^{2-}]_{\text{SW}}$ estimates ranging from < 0.1 to 70 mM , with most between ~ 1 and 16 mM . Many units exhibit combinations of $\partial\delta^{34}\text{S}_{\text{CAS}}/\partial t(\text{max})$ and $\Delta^{34}\text{S}_{\text{CAS-PY}}$ values that plot close to or slightly below the MSR trend (Fig. 6), yielding $[\text{SO}_4^{2-}]_{\text{SW}}$ estimates for the MSR-trend method that are equal to or somewhat smaller than the rate-based estimates. This pattern conforms to our expectation that the rate method yields maximum estimates of $[\text{SO}_4^{2-}]_{\text{SW}}$. The only potentially anomalous result is for the upper Huqf Supergroup, which yielded a MSR-trend estimate ($12\text{--}45\text{ mM}$) that is larger than the rate-method estimate ($1.5\text{--}8\text{ mM}$; Table S4).

We also analyzed $[\text{SO}_4^{2-}]_{\text{SW}}$ for a set of eight units of Cambrian age. These units yielded $\partial\delta^{34}\text{S}_{\text{CAS}}/\partial t(\text{max})$ of 7 to 23‰ Myr^{-1} for the early Cambrian, 9 to 20‰ Myr^{-1} for the early–middle Cambrian boundary (EMCB), and 8 to 20‰ Myr^{-1} for the late Cambrian SPICE (Table S4; Fig. 7). These ranges are sufficiently similar that they suggest a limited range of seawater $[\text{SO}_4^{2-}]$ variation during the Cambrian. The rate method yielded $[\text{SO}_4^{2-}]_{\text{SW}}$ estimates ranging from < 0.1 to 18 mM , with most between ~ 1 and 6 mM . The MSR-trend method yielded $[\text{SO}_4^{2-}]_{\text{SW}}$ estimates ranging from < 0.1 to 40 mM , with most between ~ 1 and 8 mM . The two methods thus yielded similar estimates of seawater

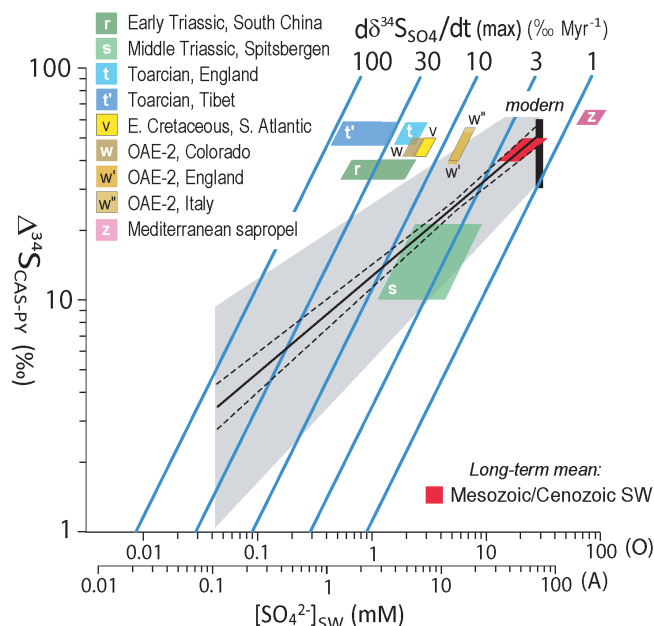


Figure 8. Analysis of seawater sulfate concentrations for eight Mesozoic–Cenozoic marine units. The parallelogram for each unit was generated using the rate method. The red field represents the long-term average $\Delta^{34}\text{S}_{\text{CAS-PY}}$ for the Mesozoic–Cenozoic based on data in Wu et al. (2010). A summary of results and data sources is given in Table S4; other details as in Figs. 1–2.

sulfate concentrations, implying that the results are reasonably robust and that the rate method is not yielding unrealistically large values. All Cambrian units show sulfate–sulfide fractionations smaller than the Paleozoic mean of 30 ± 5 ‰ (Wu et al., 2010), resulting in lower $[\text{SO}_4^{2-}]_{\text{SW}}$ estimates than for the long-term record (Fig. 4). Once again, most units exhibit combinations of $\partial\delta^{34}\text{S}_{\text{CAS}}/\partial t(\text{max})$ and $\Delta^{34}\text{S}_{\text{CAS-PY}}$ values that plot close to or slightly below the MSR trend (Fig. 7). However, two units (the SPICE events in Australia and Nevada) yield MSR-trend estimates that are larger than their rate-method estimates. The reasons for these potentially anomalous results will be considered below.

Finally, we analyzed a set of eight Mesozoic units, ranging in age from the Early Triassic to the late Middle Cretaceous (Table S4; Fig. 8). These units show $\partial\delta^{34}\text{S}_{\text{CAS}}/\partial t(\text{max})$ of 6 to 60 ‰ Myr^{−1}, with the highest rates during the Early Triassic and Early Jurassic. The rate method yielded $[\text{SO}_4^{2-}]_{\text{SW}}$ estimates ranging from 1.1 to 120 mM, with most between ~ 3 and 20 mM. The MSR-trend method yielded $[\text{SO}_4^{2-}]_{\text{SW}}$ estimates ranging from 1 to 110 mM, with most between ~ 30 and 100 mM (Table S4). In contrast to the late Neoproterozoic and Cambrian, many Mesozoic units exhibit a narrow spread of $\Delta^{34}\text{S}_{\text{CAS-PY}}$ values that conform with the mean sulfate–sulfide fractionation for the Mesozoic–Cenozoic (Wu et al., 2010; Fig. 8) and that are within the range for modern marine systems (~ 30 – 60 ‰; Table S1). As a consequence, many Mesozoic units exhibit the anomalous pattern

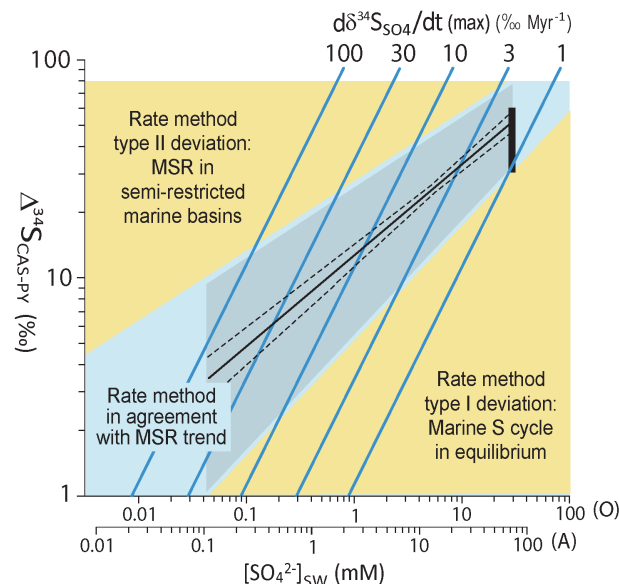


Figure 9. Interpretation of deviations in $[\text{SO}_4^{2-}]_{\text{SW}}$ estimates between the rate and MSR-trend methods. Type I deviations, in which rate-method estimates are anomalously high (lower right field), are likely to reflect extremely stable environmental conditions, in which the marine sulfur cycle is in equilibrium (i.e., balanced source and sink fluxes). Type II deviations, in which rate-based estimates are anomalously low (upper left field), are likely to reflect sulfate reduction in semi-restricted marine basins. In this case, $\Delta^{34}\text{S}_{\text{CAS-PY}}$ will be controlled by $[\text{SO}_4^{2-}]_{\text{SW}}$, which may be equal or close to that of the global ocean, but $\partial\delta^{34}\text{S}_{\text{CAS}}/\partial t(\text{max})$ will be controlled by the mass of aqueous sulfate within the restricted basin, which will be a function of basin volume.

of having MSR-trend estimates that are larger than their rate-method estimates.

Ideally, the rate and MSR-trend methods will yield similar $[\text{SO}_4^{2-}]_{\text{SW}}$ estimates, providing support for the correctness of the results, and the majority of the paleomarine units considered in this study follow this pattern. However, a subset of the study units show differences that fall into two categories: (1) type I deviation – rate-method estimates \gg MSR-trend estimates (lower right field, Fig. 9); (2) type II deviation – MSR-trend estimates \gg rate-method estimates (upper left field, Fig. 9). Such deviations may provide insights into underlying controls on seawater sulfate concentrations. The most likely explanation for the type I deviations is that the measured $\partial\delta^{34}\text{S}_{\text{CAS}}/\partial t(\text{max})$ for a given unit is much less than its theoretical maximum. This situation can develop whenever the marine sulfur cycle is in equilibrium (i.e., source and sink fluxes in balance), reflecting persistently stable environmental conditions. In this case, the rate-method estimate of $[\text{SO}_4^{2-}]_{\text{SW}}$ would have little relationship to actual $[\text{SO}_4^{2-}]_{\text{SW}}$, although the MSR-trend estimate may still be a good proxy for $[\text{SO}_4^{2-}]_{\text{SW}}$. Surprisingly, very few of the analyzed units (Table S4) show type I deviations, perhaps be-

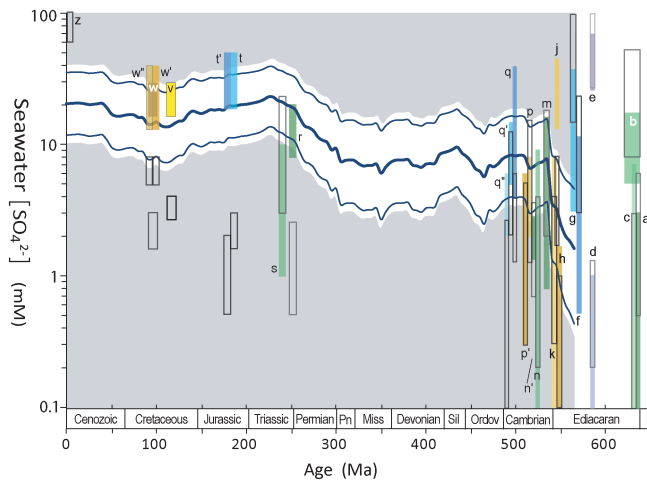


Figure 10. Seawater sulfate concentrations for late Neoproterozoic and Phanerozoic marine units (Figs. 6–8) compared with long-term $[\text{SO}_4^{2-}]_{\text{SW}}$ curve (Fig. 4). Estimates of $[\text{SO}_4^{2-}]_{\text{SW}}$ are based on (1) the rate method (calculated as per Eqs. 3 and 4; shown as open boxes) and (2) the MSR-trend method (calculated as per Eqs. 6–8; shown as solid boxes); note that unit symbols and colors are keyed to Table S4 and Figs. 6–8. See text for discussion. Other details as in Fig. 4.

cause the most heavily scrutinized ancient geologic epochs are those with unstable environments.

Type II deviations, in which $\partial\delta^{34}\text{S}_{\text{CAS}}/\partial t(\text{max})$ is anomalously high, are more common, being present in three units of late Neoproterozoic and Cambrian age (Figs. 6–7) and seven out of eight units of Mesozoic age (Fig. 8). Several factors might potentially produce this pattern. First, $\partial\delta^{34}\text{S}_{\text{CAS}}/\partial t(\text{max})$ may have been overestimated owing to inadequate geochronologic constraints, diagenetic artifacts, or analytical uncertainties in measuring $\delta^{34}\text{S}_{\text{CAS}}$. However, the fact that type II deviations are more common among Mesozoic units (Fig. 8), which are generally better dated and less diagenetically altered than older units (Figs. 6–7), suggests that such problems are relatively uncommon and unlikely to be responsible for most such anomalies. Second, the measured $\Delta^{34}\text{S}_{\text{CAS-PY}}$ for a given paleomarine unit may be unrepresentative, perhaps because of unusually large MSR fractionation (cf. Habicht et al., 2002; Canfield et al., 2010). This explanation may be applicable, for example, to Pleistocene Mediterranean sapropels (Scheiderich et al., 2010), which exhibit unusually large $\Delta^{34}\text{S}_{\text{CAS-PY}}$ values ($60 \pm 5\%$; Fig. 8). However, none of the anomalous units of late Neoproterozoic, Cambrian, or Mesozoic age exhibits a $\Delta^{34}\text{S}_{\text{CAS-PY}}$ larger than the typical modern range of ~ 30 – 60% , so elevated sulfate–sulfide fractionation is unlikely as a general explanation. We are therefore inclined to regard most type II deviations as products of local depositional conditions and to seek an environmentally based mechanism to account for them.

A possible environmental explanation for type II deviations is sulfate reduction within a restricted marine basin. In this case, $\Delta^{34}\text{S}_{\text{CAS-PY}}$ is controlled by seawater $[\text{SO}_4^{2-}]$, which may be identical (or nearly so) to that in the global ocean. However, the total mass of sulfate in the restricted marine basin will be much less than that in the global ocean, allowing a more rapid evolution of seawater sulfate $\delta^{34}\text{S}$ in response to oceanographic perturbations. We hypothesize that most of the type II deviations in our study units are the product of MSR within semi-restricted marine basins. For example, the Neoproterozoic Ara Group (Huqf Supergroup) of Oman was deposited in a fault-bounded basin in which massive evaporite deposits accumulated (Fike and Grotzinger, 2008). Also, most of the Mesozoic units showing type II deviations are known to have been deposited in basins that were subject to a degree of water mass restriction. The Triassic–Jurassic European epicontinental sea was broad, shallow, and laced with local tectonic grabens with restricted deepwater circulation (Röhl et al., 2001; Berra et al., 2010). The Early Cretaceous South Atlantic was only weakly connected to the global ocean during deposition of Aptian sediments (Wortmann and Chernyavsky, 2007), and restriction of the Atlantic Ocean continued at least through deposition of organic-rich facies at the Cenomanian–Turonian boundary (Owens et al., 2013). The Cretaceous Western Interior Seaway was almost certainly semi-restricted throughout its existence (Adams et al., 2010). The only Mesozoic unit not to show a type II deviation, the Middle Triassic Bravaisberget Formation of Spitsbergen (Karcz, 2010; Fig. 8), was deposited in the largely unrestricted Boreal Ocean. These examples serve to illustrate the need to understand the hydrography of paleomarine basins in applying the rate method of estimating paleoseawater sulfate concentrations.

Comparison of the $[\text{SO}_4^{2-}]_{\text{SW}}$ estimates for individual Neoproterozoic and Phanerozoic units shown in Figs. 6–8 with the long-term $[\text{SO}_4^{2-}]_{\text{SW}}$ curve in Fig. 4 provides additional insights regarding secular variation in seawater sulfate inventories. With the exception of the Middle Triassic Bravaisberget Formation, all Mesozoic units exhibit MSR-trend estimates that overlap the long-term trend but rate estimates that fall below it (Fig. 10). As discussed above, we infer that this pattern reflects anomalously high measured $\partial\delta^{34}\text{S}_{\text{CAS}}/\partial t(\text{max})$ values as a consequence of rapid evolution of seawater sulfate $\delta^{34}\text{S}$ within semi-restricted marine basins of the proto-Atlantic and western Tethys oceans. Cambrian units exhibit a wide range of $[\text{SO}_4^{2-}]_{\text{SW}}$ estimates, although a cluster of results falls just below the long-term trend, with many estimates between 1 and 5 mM (Fig. 10). We infer that either our long-term record (Fig. 4) overestimates $[\text{SO}_4^{2-}]_{\text{SW}}$ for the Cambrian, or the studied units are biased toward low $[\text{SO}_4^{2-}]_{\text{SW}}$. Late Neoproterozoic units exhibit an even wider range of $[\text{SO}_4^{2-}]_{\text{SW}}$ estimates than Cambrian units and lack any apparent clustering (Fig. 10). However, all but one of these units yield similar $[\text{SO}_4^{2-}]_{\text{SW}}$ es-

estimates for the MSR-trend and rate methods (Fig. 6), suggesting that the estimates are robust. We infer that the late Neoproterozoic (635–542 Ma) was characterized by a highly unstable marine sulfur cycle, as a consequence of which seawater sulfate concentrations varied tremendously. This inference is supported by some earlier studies (Li et al., 2010; Loyd et al., 2012, 2013), although other studies have inferred low (Hurtgen et al., 2002, 2005, 2006; Ries et al., 2009) or monotonically rising sulfate concentrations (Halverson and Hurtgen, 2007) during this interval.

5 Conclusions

The rate and MSR-trend methods developed in this study for quantifying paleo-seawater sulfate concentrations are complementary and quasi-independent, providing estimates of maximum and mean $[\text{SO}_4^{2-}]_{\text{sw}}$, respectively, for a paleomarine unit of interest. Both techniques make use of $\Delta^{34}\text{S}_{\text{CAS-PY}}$, i.e., the isotopic fractionation associated with microbial sulfate reduction (MSR). The rate method evaluates $[\text{SO}_4^{2-}]_{\text{sw}}$ as a function of $\partial\delta^{34}\text{S}_{\text{CAS}}/\partial t(\text{max})$, i.e., the maximum observed rate of change in seawater sulfate, whereas the MSR-trend method makes use of an empirical relationship between MSR fractionation and aqueous sulfate concentrations. The significance of our quantitative approach is that estimates of paleo-seawater $[\text{SO}_4^{2-}]$ can be derived from two readily measurable sedimentary parameters: $\Delta^{34}\text{S}_{\text{CAS-PY}}$ and $\partial\delta^{34}\text{S}_{\text{CAS}}/\partial t(\text{max})$. Based on these methods, an analysis of long-term variation since 635 Ma suggests that $[\text{SO}_4^{2-}]_{\text{sw}}$ was low during the late Neoproterozoic (< 5 mM), rose sharply across the Ediacaran–Cambrian boundary (to ~ 5 – 10 mM), and rose again during the Permian to near-modern levels (~ 10 – 30 mM). However, high-resolution $\delta^{34}\text{S}_{\text{CAS}}$ studies provide evidence of episodic high-frequency ($< \sim 2$ Myr) events during which seawater sulfate concentrations were drawn down in response to massive evaporite deposition, reduced sediment ventilation and increased pyrite burial in the aftermath of mass extinctions, or other factors. The techniques developed in this study for quantitative analysis of paleo-seawater $[\text{SO}_4^{2-}]$ should be applicable to marine units of any age provided that (1) MSR fractionation has been a conservative process through time (i.e., the dominant pathways of sulfur metabolism have not changed greatly) and (2) sufficient time control exists for estimation of rates of $\delta^{34}\text{S}_{\text{CAS}}$ variation. As more S-isotopic studies of cogenetic sulfate and sulfide become available, it should ultimately be possible to reconstruct variation in seawater sulfate concentrations throughout Earth history.

Appendix A: Extended discussion

A1 Relationship of rate of seawater sulfate change to sulfate residence time

The maximum possible rate of change in seawater sulfate $\delta^{34}\text{S}$ (i.e., $\partial\delta^{34}\text{S}_{\text{SO}_4}/\partial t(\text{max})$) is inversely proportional to the residence time of sulfate in seawater (τ). The exact quantitative form of this relationship can be derived from Eq. (2) of Algeo et al. (2014), reorganization of which yields

$$M_{\text{SW}}/F_{\text{PY}} = k_1 \times \Delta^{34}\text{S}_{\text{CAS-PY}}/\partial\delta^{34}\text{S}_{\text{CAS}}/\partial t(\text{max}). \quad (\text{A1})$$

The residence time of sulfur in seawater is equal to the mass of seawater sulfate divided by the total sink flux, i.e., the reduced sulfur flux (F_{PY}) plus the oxidized sulfur flux (F_{EVAP}):

$$\tau = M_{\text{SW}}/(F_{\text{PY}} + F_{\text{EVAP}}). \quad (\text{A2})$$

If we let φ_{PY} be the fraction of the total S flux represented by pyrite burial (i.e., $F_{\text{PY}}/(F_{\text{PY}} + F_{\text{EVAP}})$), then

$$\tau \times \varphi_{\text{PY}}^{-1} = M_{\text{SW}}/F_{\text{PY}}, \quad (\text{A3})$$

and substitution into Eq. (A1) yields

$$\tau \times \varphi_{\text{PY}}^{-1} = k_1 \times \Delta^{34}\text{S}_{\text{CAS-PY}}/\partial\delta^{34}\text{S}_{\text{CAS}}/\partial t(\text{max}). \quad (\text{A4})$$

This equation quantifies the inverse proportionality between the maximum rate of change of seawater sulfate $\delta^{34}\text{S}$ and the residence time of sulfur in seawater.

A2 Effects of $[\text{SO}_4^{2-}]_{\text{SW}}$ -dependent pyrite burial fluxes on $[\text{SO}_4^{2-}]_{\text{SW}}$ estimates

Although we made use of fixed estimates of the pyrite burial flux (F_{PY}), i.e., $4 \times 10^{13} \text{ g yr}^{-1}$ for oxic oceans and $10 \times 10^{13} \text{ g yr}^{-1}$ for anoxic oceans, it is possible that F_{PY} is dependent on $[\text{SO}_4^{2-}]_{\text{SW}}$. Wortmann and Chernyavsky (2007) inferred a nonlinear positive relationship of F_{PY} with $[\text{SO}_4^{2-}]_{\text{SW}}$ (their Fig. 4). We explored the effects of varying pyrite burial fluxes on seawater sulfate estimates as follows. Equations (2–3) have four variables: $[\text{SO}_4^{2-}]_{\text{SW}}$ (or M_{SW} , since these are interconvertible via Eq. 4), F_{PY} , $\Delta^{34}\text{S}_{\text{CAS-PY}}$, and $\partial\delta^{34}\text{S}_{\text{SO}_4}/\partial t$. However, $\Delta^{34}\text{S}_{\text{CAS-PY}}$ can be modeled as a function of $[\text{SO}_4^{2-}]_{\text{SW}}$ (i.e., the MSR trend of Fig. 2 and Eq. 6), reducing the number of potentially independent variables to three (we state “potentially independent” as there may in fact be some dependency among these variables). Now it is possible to explore the effects of simultaneous variations in $[\text{SO}_4^{2-}]_{\text{SW}}$ and F_{PY} on $\partial\delta^{34}\text{S}_{\text{SO}_4}/\partial t(\text{max})$ via a modified form of Eq. (2):

$$\begin{aligned} \partial\delta^{34}\text{S}_{\text{CAS}}/\partial t(\text{max}) &= k_1 \times k_2 \times F_{\text{PY}} \\ &\times \exp(\log[\text{SO}_4^{2-}]_{\text{SW}} \times 0.42 + 1.10)/[\text{SO}_4^{2-}]_{\text{SW}}. \end{aligned} \quad (\text{A5})$$

The three modeled parameters exhibit log-linear relationships, with larger $\partial\delta^{34}\text{S}_{\text{CAS}}/\partial t(\text{max})$ associated with larger

Table A1. Regression statistics for reduced sulfur phases (0–40 PSU only; see Fig. A3).

Sulfur phase	n	r	m	b	$p(\alpha)$
Pyrite	48	0.92	0.46	−0.35	< 0.01
Sediment AVS	6	0.81	0.42	−0.06	< 0.05
Sediment TRS	11	0.89	0.33	0.20	< 0.01
Aqueous H_2S	16	0.84	0.44	−0.20	< 0.01

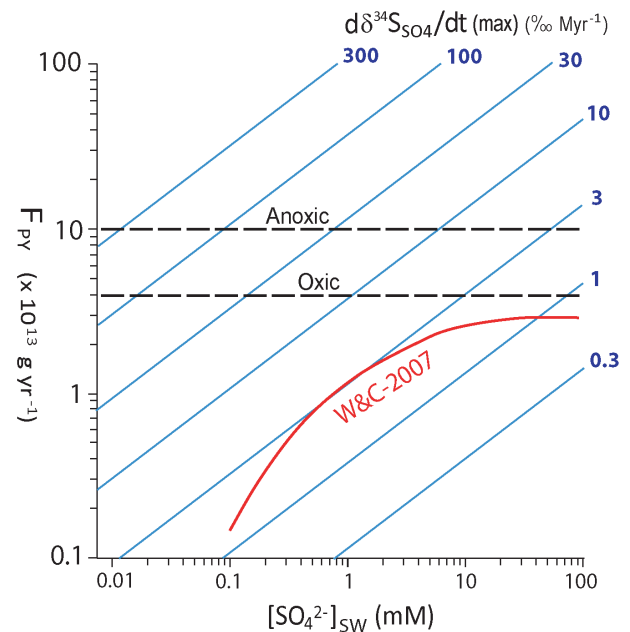


Figure A1. Relationship of $\partial\delta^{34}\text{S}_{\text{CAS}}/\partial t(\text{max})$ to F_{PY} and $[\text{SO}_4^{2-}]_{\text{SW}}$, with $\Delta^{34}\text{S}_{\text{CAS-PY}}$ estimated as a function of $[\text{SO}_4^{2-}]_{\text{SW}}$ (Fig. 2, Eq. 6). The dashed horizontal lines represent the pyrite burial fluxes used in this study for oxic and anoxic paleo-marine systems, i.e., 4×10^{13} and $10 \times 10^{13} \text{ g yr}^{-1}$, respectively. The red line represents the $[\text{SO}_4^{2-}]_{\text{SW}}$ dependency of the pyrite burial flux as given by Wortmann and Chernyavsky (2007, their Fig. 4). Note that, according to the latter relationship, $\partial\delta^{34}\text{S}_{\text{CAS}}/\partial t(\text{max})$ values cannot exceed $\sim 3 \text{ ‰ Myr}^{-1}$ under any set of conditions.

$[\text{SO}_4^{2-}]_{\text{SW}}$ and F_{PY} (Fig. A1). $\partial\delta^{34}\text{S}_{\text{CAS}}/\partial t(\text{max})$ scales linearly with F_{PY} , so uncertainty in the latter parameter is directly mirrored in the former parameter. The range of F_{PY} used in our study (i.e., $4\text{--}10 \times 10^{13} \text{ g yr}^{-1}$) is consistent with variation in $\partial\delta^{34}\text{S}_{\text{CAS}}/\partial t(\text{max})$ from ~ 1 to 100 ‰ Myr^{-1} . The $F_{\text{PY}}\text{--}[\text{SO}_4^{2-}]_{\text{SW}}$ relationship of Wortmann and Chernyavsky (2007, their Fig. 4; red curve, Fig. A1), if correct, indicates that variation in $\partial\delta^{34}\text{S}_{\text{CAS}}/\partial t(\text{max})$ cannot exceed $\sim 3 \text{ ‰ Myr}^{-1}$ under any set of conditions.

We tested the influence of sulfate-dependent pyrite burial fluxes on seawater sulfate concentration estimates by applying the relationship of Wortmann and Chernyavsky (2007) to our rate-method calculations. Their relationship can be re-

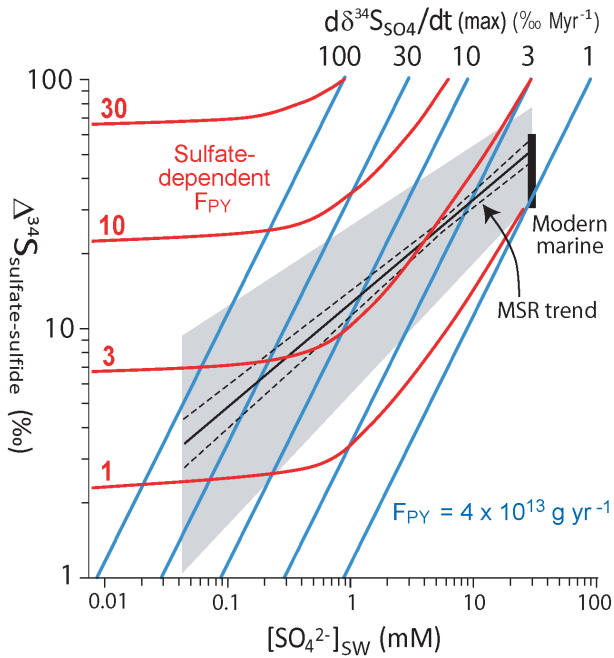


Figure A2. $\partial\delta^{34}S_{CAS} / \partial t(\max)$ values calculated using fixed pyrite burial fluxes (blue diagonal lines; cf. Fig. 1) and the sulfate-dependent pyrite burial fluxes of Wortmann and Chernyavsky (2007; red curves). Note that, for the latter curves, many combinations of the two measured sediment parameters ($\Delta^{34}S_{CAS-PY}$ and $\partial\delta^{34}S_{CAS} / \partial t(\max)$) cannot yield a $[SO_4^{2-}]_{SW}$ estimate. Shown for reference is the MSR trend of Fig. 2.

duced to a logarithmic expression:

$$F_{PY} = 0.7681 \times \ln([SO_4^{2-}]_{SW}) + 1.405, \quad (A6)$$

where F_{PY} is in units of $10^{13} \text{ g yr}^{-1}$ (rather than in mol yr^{-1} , as in their paper) and $[SO_4^{2-}]_{SW}$ is in units of millimoles. This expression yielded an r^2 of 0.98 in relation to Wortmann and Chernyavsky's curve (their Fig. 4). In making use of sulfate-dependent pyrite burial fluxes for calculation of seawater sulfate concentration estimates, Eqs. (3) and (4) must be reorganized as follows:

$$[SO_4^{2-}]_{SW}(\max) / F_{PY} = k_1 \times k_2 \times \Delta^{34}S_{CAS-PY} / \partial\delta^{34}S_{CAS} / \partial t(\max). \quad (A7)$$

Although Eq. (A7) has two unknowns, i.e., $[SO_4^{2-}]_{SW}(\max)$ and F_{PY} , it can be solved because F_{PY} is a function of $[SO_4^{2-}]_{SW}$ in Fig. 4 of Wortmann and Chernyavsky (2007). The empirical relationship between $[SO_4^{2-}]_{SW}$ and

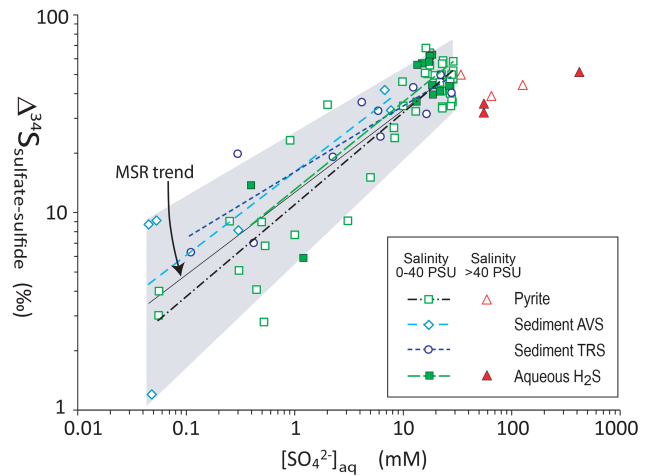


Figure A3. Replotted MSR-trend data (from Fig. 2, Table S1) as a function of sulfide $\delta^{34}S$ source (symbols as given in legend). Separate regressions for the four different sulfide phases (dashed lines; calculated for 0–40 PSU only) show small differences in slopes and y intercepts (Table A1), although the regression lines are statistically indistinguishable.

$[SO_4^{2-}]_{SW}(\max) / F_{PY}$ is given by the polynomial equation

$$[SO_4^{2-}]_{SW}(\max) / F_{PY} = -0.0018([SO_4^{2-}]_{SW})^2 + 0.2842([SO_4^{2-}]_{SW}) + 0.4651. \quad (A8)$$

With substitution and reorganization, Eqs. (A7) and (A8) yield

$$0 = -0.0018([SO_4^{2-}]_{SW})^2 + 0.2842([SO_4^{2-}]_{SW}) + \left(0.4651 - k_1 \times k_2 \times \Delta^{34}S_{CAS-PY} / [\partial\delta^{34}S_{CAS} / \partial t(\max)]\right). \quad (A9)$$

This second-order polynomial equation can now be solved for $[SO_4^{2-}]_{SW}$ using the quadratic solution, after which F_{PY} can be calculated from Eq. (A6).

Using Eq. (A9), we calculated $[SO_4^{2-}]_{SW}$ on the basis of $\partial\delta^{34}S_{CAS} / \partial t(\max)$ and $\Delta^{34}S_{CAS-PY}$. These relationships are plotted as variation in $\partial\delta^{34}S_{CAS} / \partial t(\max)$ as a function of $[SO_4^{2-}]_{SW}$ and $\Delta^{34}S_{CAS-PY}$ (Fig. A2; cf. Fig. 1). At high $[SO_4^{2-}]_{SW}$, the two sets of $\partial\delta^{34}S_{CAS} / \partial t(\max)$ curves are nearly colinear, which is because the value of F_{PY} in Fig. 4 of Wortmann and Chernyavsky (2007) for $[SO_4^{2-}]_{SW} > 10 \text{ mM}$ is nearly invariant and similar to the flux that we used for oxic marine environments (i.e., $4 \times 10^{13} \text{ g yr}^{-1}$). In contrast, the two sets of curves diverge sharply at $[SO_4^{2-}]_{SW} < 1 \text{ mM}$, which is a consequence of the much lower F_{PY} values associated with low seawater sulfate concentrations in the Wortmann and Chernyavsky curve.

The $\partial\delta^{34}S_{CAS} / \partial t(\max)$ curves based on the sulfate-dependent pyrite fluxes of Wortmann and

Chernyavsky (2007) require comment. First, the MSR trend (Fig. 2) corresponds almost entirely to a limited range of $\partial\delta^{34}\text{S}_{\text{CAS}}/\partial t(\text{max})$ values (i.e., 2 to 4‰ Myr⁻¹; Fig. A2). This suggests that there ought to be quite limited variation in $\partial\delta^{34}\text{S}_{\text{CAS}}/\partial t(\text{max})$ over a wide range of seawater sulfate concentrations in nature. Second, many combinations of the two sediment parameters that can be measured (i.e., $\Delta^{34}\text{S}_{\text{CAS-PY}}$ and $\partial\delta^{34}\text{S}_{\text{CAS}}/\partial t(\text{max})$) cannot yield a $[\text{SO}_4^{2-}]_{\text{SW}}$ estimate. For example, no $[\text{SO}_4^{2-}]_{\text{SW}}$ estimate is possible for $\Delta^{34}\text{S}_{\text{CAS-PY}}$ of 7‰ in combination with any $\partial\delta^{34}\text{S}_{\text{CAS}}/\partial t(\text{max})$ value that is larger than ~ 4 ‰ Myr⁻¹ (Fig. B2). This situation exists because high rates of variation in seawater sulfate $\delta^{34}\text{S}$ are not possible where the pyrite burial flux is sharply curtailed by $[\text{SO}_4^{2-}]_{\text{SW}}$ dependency (as in Fig. 4 of Wortmann and Chernyavsky, 2007). However, many paleomarine units exhibit $\partial\delta^{34}\text{S}_{\text{CAS}}/\partial t(\text{max})$ values outside the narrow range permitted by the Wortmann and Chernyavsky (2007) relationship (see Table S4 and Figs. 6–8). If the Wortmann and Chernyavsky (2007) parameterization of the $F_{\text{PY}}-[\text{SO}_4^{2-}]_{\text{SW}}$ relationship is correct, then one must conclude that all of these published higher rates are products of uncertain geochronologic dating, diagenetic artifacts, or sample processing and analytical problems. On the other hand, the use of fixed values for F_{PY} in our rate-method calculations (Eqs. 2–4) yields estimates of $[\text{SO}_4^{2-}]_{\text{SW}}$ that are – for the most part – consistent with estimates of $[\text{SO}_4^{2-}]_{\text{SW}}$ based on the MSR-trend method (Sect. 2.2; see Figs. 6–8 for examples). We acknowledge that some form of sulfate dependency of pyrite burial fluxes may exist but suggest that it may differ from the relationship given by Wortmann and Chernyavsky (2007).

A3 Sources of sulfide $\delta^{34}\text{S}$ data

Although all sulfate $\delta^{34}\text{S}$ data used in the calculation of $\Delta^{34}\text{S}_{\text{sulfate-sulfide}}$ values in Fig. 2 are based on aqueous SO_4^{2-} measurements, we used sulfide $\delta^{34}\text{S}$ data from multiple sources: pyrite, sediment acid-volatile sulfur (AVS), sediment total reduced sulfur (TRS), and aqueous H_2S (Table S1). We have constructed a version of Fig. 2 that shows the different sulfide phases, and we calculated separate regressions for each phase (Fig. A3). The following points should be noted about this figure. First, each of the four phases yields a statistically significant regression ($r = 0.81$ – 0.92 ; $p(\alpha) < 0.05$; Table A1). Second, the four phases have similar regression slopes although slightly variable y intercepts. For this reason, TRS and AVS yield $\Delta^{34}\text{S}_{\text{CAS-PY}}$ values that are, on average, slightly larger for a given $[\text{SO}_4^{2-}]_{\text{SW}}$ than pyrite and aqueous H_2S . Third, the four regression lines generally converge at higher $[\text{SO}_4^{2-}]_{\text{SW}}$, and the largest differences occur at low $[\text{SO}_4^{2-}]_{\text{SW}}$, where data are sparser.

One point that bears reflection is that estimates of paleo-seawater $[\text{SO}_4^{2-}]_{\text{SW}}$ are based not on aqueous sulfide $\delta^{34}\text{S}$, which cannot be measured for paleomarine systems, but on mineral sulfide (generally pyrite) $\delta^{34}\text{S}$. Therefore, the critical relationship for establishing a viable MSR-trend proxy for $[\text{SO}_4^{2-}]_{\text{SW}}$ is that between sulfate $\delta^{34}\text{S}$ and pyrite $\delta^{34}\text{S}$. Although we could have used the pyrite $\delta^{34}\text{S}$ data alone, we opted to include other sulfide phases to produce a larger sulfide $\delta^{34}\text{S}$ data set, especially one containing more data at low $[\text{SO}_4^{2-}]_{\text{SW}}$, with the goal of generating a stable relationship over a wider range of $[\text{SO}_4^{2-}]_{\text{SW}}$ values. Whether there are real differences in the regression relationships among these four sulfide phases is an issue that will require further inquiry. These sulfide phases yield similar relationships between $\Delta^{34}\text{S}_{\text{sulfate-sulfide}}$ and $[\text{SO}_4^{2-}]_{\text{SW}}$ that, based on the available data, are statistically indistinguishable (Fig. A3).

The Supplement related to this article is available online at doi:10.5194/bg-12-2131-2015-supplement.

Author contributions. T. J. Algeo developed the project concept and modeling methodology; G. M. Luo, H. Y. Song, T. W. Lyons, and D. E. Canfield provided isotopic data; and all authors assisted in drafting the manuscript.

Acknowledgements. We thank U. G. Wortmann and an anonymous reviewer for constructive reviews and C. P. Slomp for editorial handling of the manuscript. Research by T. J. Algeo and T. W. Lyons is supported by the Sedimentary Geology and Paleobiology program of the US National Science Foundation and the NASA Exobiology program. T. J. Algeo also gratefully acknowledges support from the China University of Geosciences, Wuhan (SKL-GPMR program GPMR201301, and SKL-BGEG program BGL21407).

Edited by: C. P. Slomp

References

- Adams, D. D., Hurtgen, M. T., and Sageman, B. B.: Volcanic triggering of a biogeochemical cascade during Oceanic Anoxic Event 2, *Nat. Geosci.*, 3, 201–204, 2010.
- Algeo, T. J., Meyers, P. A., Robinson, R. S., Rowe, H., and Jiang, G. Q.: Icehouse-greenhouse variations in marine denitrification, *Biogeosciences*, 11, 1273–1295, doi:10.5194/bg-11-1273-2014, 2014.
- Asmussen, G. and Strauch, G.: Sulfate reduction in a lake and the groundwater of a former lignite mining area studied by stable sulfur and carbon isotopes, *Water Air Soil Poll.*, 108, 271–284, 1998.
- Bates, A. L., Spiker, E. C., Orem, W. H., and Burnett, W. C.: Speciation and isotopic composition of sulfur in sediments from Jellyfish Lake, Palau, *Chem. Geol.*, 106, 63–76, 1993.
- Bates, A. L., Spiker, E. C., Hatcher, P. G., Stout, S. A., and Weintraub, V. C.: Sulfur geochemistry of organic-rich sediments from Mud Lake, Florida, USA, *Chem. Geol.*, 121, 245–262, 1995.
- Bates, A. L., Spiker, E. C., and Holmes, C. W.: Speciation and isotopic composition of sedimentary sulfur in the Everglades, Florida, USA, *Chem. Geol.*, 146, 155–170, 1998.
- Bekker, A., Holland, H. D., Wang, P. L., Rumble, D., III, Stein, H. J., Hannah, J. L., Coetzee, L. L., and Beukes, N. J.: Dating the rise of atmospheric oxygen, *Nature*, 427, 117–120, 2004.
- Bergman, N. M., Lenton, T. M., and Watson, A. J.: COPSE: a new model of biogeochemical cycling over Phanerozoic time, *Am. J. Sci.*, 397–437, 2004.
- Berner, R. A.: A model for calcium, magnesium and sulfate in seawater over Phanerozoic time, *Am. J. Sci.*, 304, 438–453, 2004.
- Berner, Z. A., Puchelt, H., Nöltner, T., and Kramar, U.: Pyrite geochemistry in the Toarcian Posidonia Shale of southwest Germany: evidence for contrasting trace-element patterns of diagenetic and syngenetic pyrites, *Sedimentology*, 60, 548–573, 2013.
- Berra, F., Jadoul, F., and Anelli, A.: Environmental control on the end of the Dolomia Principale/Hauptdolomit depositional system in the central Alps: coupling sea-level and climate changes, *Palaeogeogr. Palaeoclimatol. Palaeoecol.*, 290, 138–150, 2010.
- Böttcher, M. E., Voss, M., Schulz-Bull, D., Schneider, R., Leipe, T., and Knöller, K.: Environmental changes in the Pearl River Estuary (China) as reflected by light stable isotopes and organic contaminants, *J. Mar. Syst.*, 82, S43–S53, 2010.
- Bottrell, S. H. and Newton, R. J.: Reconstruction of changes in global sulfur cycling from marine sulfate isotopes, *Earth-Sci. Rev.*, 75, 59–83, 2006.
- Bradley, A. S., Leavitt, W. D., and Johnston, D. T.: Revisiting the dissimilatory sulfate reduction pathway, *Geobiology*, 9, 446–457, 2011.
- Brennan, S. T., Lowenstein, T. K., and Horita, J.: Seawater chemistry and the advent of biocalcification, *Geology*, 32, 473–476, 2004.
- Brüchert, V.: Physiological and ecological aspects of sulfur isotope fractionation during bacterial sulfate reduction, in: *Sulfur Biogeochemistry – Past and Present*, edited by: Amend, J. P., Edwards, K. J., and Lyons, T. W., *Geol. Soc. Am. Spec. Pap.*, 379, 1–16, 2004.
- Brüchert, V. and Pratt, L. M.: Contemporaneous early diagenetic formation of organic and inorganic sulfur in estuarine sediments from St. Andrew Bay, Florida, USA, *Geochim. Cosmochim. Ac.*, 60, 2325–2332, 1996.
- Brüchert, V. and Pratt, L. M.: Stable sulfur isotopic evidence from historical changes of sulfur cycling in estuarine sediments from northern Florida, *Aquat. Geochem.*, 5, 249–268, 1999.
- Brüchert, V., Knoblauch, C., and Jørgensen, B. B.: Microbial controls on the stable sulfur isotope fractionation during bacterial sulfate reduction in Arctic sediments, *Geochim. Cosmochim. Ac.*, 65, 753–766, 2001.
- Brunner, B. and Bernasconi, S. M.: A revised isotope fractionation model for dissimilatory sulfate reduction in sulfate-reducing bacteria, *Geochim. Cosmochim. Ac.*, 69, 4759–4771, 2005.
- Canfield, D. E.: A new model for Proterozoic ocean chemistry, *Nature*, 396, 450–453, 1998.
- Canfield, D. E.: Isotope fractionation by natural populations of sulfate-reducing bacteria, *Geochim. Cosmochim. Ac.*, 65, 1117–1124, 2001.
- Canfield, D. E.: The evolution of the Earth surface sulfur reservoir, *Am. J. Sci.*, 304, 839–861, 2004.
- Canfield, D. E. and Farquhar, J.: Animal evolution, bioturbation, and the sulfate concentration of the oceans, *Proc. Nat. Acad. Sci. (USA)*, 106, 8123–8127, 2009.
- Canfield, D. E. and Raiswell, R.: The evolution of the sulfur cycle, *Am. J. Sci.*, 299, 697–723, 1999.
- Canfield, D. E. and Thamdrup, B. T.: The production of ^{34}S -depleted sulfide during disproportionation of elemental sulfur, *Science*, 266, 1973–1975, 1994.
- Canfield, D. E., Raiswell, R., and Bottrell, S.: The reactivity of sedimentary iron minerals toward sulfide, *Am. J. Sci.*, 292, 659–683, 1992.
- Canfield, D. E., Olesen, C. A., and Cox, R. P.: Temperature and its control of isotope fractionation by a sulfate-reducing bacterium, *Geochim. Cosmochim. Ac.*, 70, 548–561, 2006.

- Canfield, D. E., Poulton, S. W., and Narbonne, G. M.: Late-Neoproterozoic deep-ocean oxygenation and the rise of animal life, *Science*, 315, 92–95, 2007.
- Canfield, D. E., Farquhar, J., and Zerkle, A. L.: High isotope fractionations during sulfate reduction in a low-sulfate euxinic ocean analog, *Geology*, 38, 415–418, 2010.
- Chambers, L. A., Trudinger, P. A., Smith, J. W., and Burns, M. S.: Fractionation of sulfur isotopes by continuous cultures of *Desulfovibrio desulfuricans*, *Can. J. Microbiol.*, 21, 1602–1607, 1975.
- Chanton, J. P. and Lewis, F. G.: Plankton and dissolved inorganic carbon isotopic composition in a river-dominated estuary: Apalachicola Bay, Florida, *Estuaries*, 22, 575–583, 1999.
- Detmers, J., Brüchert, V., Habicht, K. S., and Kuever, J.: Diversity of sulfur isotope fractionations by sulfate-reducing prokaryotes, *Appl. Environ. Microbiol.*, 67, 888–894, 2001.
- DiMichele, W. A. and Hook, R. W.: Paleozoic terrestrial ecosystems, in: *Terrestrial Ecosystems through Time*, edited by: Behrensmeyer, A. K., Damuth, J. D., DiMichele, W. A., Potts, R., Sues, H.-D., and Wing, S. L., The University of Chicago Press, 205–325, 1992.
- Doi, H., Kikuchi, E., Mizota, C., Satoh, N., Shikano, S., Yurlova, N., Yadrenkina, E., and Zuykova, E.: Carbon, nitrogen, and sulfur isotope changes and hydro-geological processes in a saline lake chain, *Hydrobiologia*, 529, 225–235, 2004.
- Eckert, T., Brunner, B., Edwards, E. A., and Wortmann, U.G.: Microbially mediated re-oxidation of sulfide during dissimilatory sulfate reduction by *Desulfobacter latus*, *Geochim. Cosmochim. Ac.*, 75, 3469–3485, 2011.
- Farquhar, J., Peters, M., Johnston, D. T., Strauss, H., Masterson, A., Wiechert, U., and Kaufman, A. J.: Isotopic evidence for Mesoproterozoic anoxia and changing atmospheric sulphur chemistry, *Nature*, 449, 706–710, 2007.
- Fike, D. A. and Grotzinger, J. P.: A paired sulfate-pyrite $\delta^{34}\text{S}$ approach to understanding the evolution of the Ediacaran-Cambrian sulfur cycle, *Geochim. Cosmochim. Ac.*, 72, 2636–2648, 2008.
- Fike, D. A., Grotzinger, J. P., Pratt, L. M., and Summons, R. E.: Oxidation of the Ediacaran Ocean, *Nature*, 444, 744–747, 2006.
- Fry, B.: Sources of carbon and sulfur nutrition for consumers in three meromictic lakes of New York State, *Limnol. Oceanogr.*, 31, 79–88, 1986a.
- Fry, B.: Stable sulfur isotopic distributions and sulfate reduction in lake sediments of the Adirondacks Mountains, New York, *Biogeochemistry*, 2, 329–343, 1986b.
- Fry, B., Giblin, A., and Dornblaser, M.: Stable sulfur isotopic compositions of chromium-reducible sulfur in lake sediments, in: *Geochemical Transformation of Sedimentary Sulfur*, edited by: Vairavamurthy, A. and Schoonens, M. A. A., American Chemical Society, ACS Symposium Series, 612, 397–410, 1995.
- Fry, B., Jannasch, H. W., Molyneaux, S. J., Wirsén, C. O., Muramoto, J. A., and King, S.: Stable isotope studies of the carbon, nitrogen and sulfur cycles in the Black Sea and the Cariaco Trench, *Deep-Sea Res.*, A38 (Suppl. 2), S1003–S1019, 1991.
- Gellatly, A. M. and Lyons, T. W.: Trace sulfate in mid-Proterozoic carbonates and the sulfur isotope record of biospheric evolution, *Geochim. Cosmochim. Ac.*, 69, 3813–3829, 2005.
- Gill, B. C., Lyons, T. W., and Saltzman, M. R.: Parallel, high-resolution carbon and sulfur isotope records of the evolving Paleozoic marine sulfur reservoir, *Palaeogeogr. Palaeoclimatol. Palaeoecol.*, 256, 156–173, 2007.
- Gill, B. C., Lyons, T. W., Young, S. A., Kump, L. R., Knoll, A. H., and Saltzman, M. R.: Geochemical evidence for widespread euxinia in the Later Cambrian ocean, *Nature*, 469, 80–83, 2011a.
- Gill, B. C., Lyons, T. W., and Jenkyns, H. C.: A global perturbation to the sulfur cycle during the Toarcian Oceanic Anoxic Event, *Earth Planet. Sci. Lett.*, 312, 484–496, 2011b.
- Gomes, M. L. and Hurtgen, M. T.: Sulfur isotope systematics of a euxinic, low-sulfate lake: evaluating the importance of the reservoir effect in modern and ancient oceans, *Geology*, 41, 663–666, 2013.
- Gorlenko, V. M. and Chebotarev, E. N.: Microbiologic processes in meromictic Lake Sakovo, *Microbiology*, 50, 134–139, 1981.
- Gorlenko, V. M., Vainstein, B., and Kachalkin, V. I.: Microbiological characteristic of Lake Mogilnoe, *Arch. Hydrobiol.*, 81, 475–492, 1978.
- Gradstein, F. M., Ogg, J. G., Schmitz, M. D., and Ogg, G. M.: *The Geologic Time Scale 2012*, Elsevier, Amsterdam, 2, 1176 pp., 2012.
- Habicht, K. S. and Canfield, D. E.: Sulphur isotope fractionation in modern microbial mats and the evolution of the sulphur cycle, *Nature*, 382, 342–343, 1996.
- Habicht, K. S. and Canfield, D. E.: Sulfur isotope fractionation during bacterial sulfate reduction in organic-rich sediments, *Geochim. Cosmochim. Ac.*, 61, 5351–5361, 1997.
- Habicht, K. S. and Canfield, D. E.: Isotope fractionation by sulfate-reducing natural populations and the isotopic composition of sulfide in marine sediments, *Geology*, 29, 555–558, 2001.
- Habicht, K. S., Gade, M., Thamdrup, B., Berg, P., and Canfield, D. E.: Calibration of sulfate levels in the Archean ocean, *Science*, 298, 2372–2374, 2002.
- Halevy, I., Peters, S. E., and Fischer, W. W.: Sulfate burial constraints on the Phanerozoic sulfur cycle, *Science*, 337, 331–334, 2012.
- Halverson, G. P. and Hurtgen, M. T.: Ediacaran growth of the marine sulfate reservoir, *Earth Planet. Sci. Lett.*, 263, 32–44, 2007.
- Halverson, G. P., Hoffman, P. F., Schrag, D. P., Maloof, A. C., and Rice, A. H. N.: Toward a Neoproterozoic composite carbon-isotope record, *Geol. Soc. Am. Bull.*, 117, 1181–1207, 2005.
- Hartmann, M. and Nielsen, H.: $\delta^{34}\text{S}$ -Werte in rezenten Meeressedimenten und ihre Deutung am Beispiel einiger Sedimentprofile aus der westlichen Ostsee, *Geol. Rundsch.*, 58, 621–655, 1968.
- Holland, H. D.: Volcanic gases, black smokers, and the Great Oxidation Event, *Geochim. Cosmochim. Ac.*, 66, 3811–3826, 2002.
- Holser, W., Maynard, J. B., and Cruikshank, K.: Modelling the natural cycle of sulphur through Phanerozoic time, in: *Evolution of the Global Biogeochemical Sulfur Cycle*, edited by: Brimblecombe, P. and Lein, A. Y. Wiley, New York, 21–56, 1989.
- Horita, J., Zimmermann, H., and Holland, H. D.: Chemical evolution of seawater during the Phanerozoic: Implications from the record of marine evaporites, *Geochim. Cosmochim. Ac.*, 66, 3733–3756, 2002.
- Hurtgen, M. T., Arthur, M. A., Suits, N. S., and Kaufman, A. J.: The sulfur isotopic composition of Neoproterozoic seawater sulfate: implications for a snowball Earth?, *Earth Planet. Sci. Lett.*, 203, 413–429, 2002.
- Hurtgen, M. T., Arthur, M. A., and Halverson, G. P.: Neoproterozoic sulfur isotopes, the evolution of microbial sulfur species, and the

- burial efficiency of sulfide as sedimentary pyrite, *Geology*, 33, 41–44, 2005.
- Hurtgen, M. T., Halverson, G. P., Arthur, M. A., and Hoffman, P. F.: Sulfur cycling in the aftermath of a 635 Ma snowball glaciation: Evidence for a syn-glacial sulfidic deep ocean, *Earth Planet. Sci. Lett.*, 245, 551–570, 2006.
- Ivanov, M. V., Rusanov, I. I., Pimenov, N. V., Bairamov, I. T., Yusupov, S. K., Savvichev, A. S., Lein, A. Y., and Sapozhnikov, V. V.: Microbial processes of the carbon and sulfur cycles in Lake Mogil'noe, *Microbiology*, 70, 583–593, 2001.
- Johnston, D. T.: Multiple sulfur isotopes and the evolution of Earth's surface sulfur cycle, *Earth-Sci. Rev.*, 106, 161–183, 2011.
- Johnston, D. T., Wing, B. A., Farquhar, J., Kaufman, A. J., Strauss, H., Lyons, T. W., Kah, L. C., and Canfield, D. E.: Active microbial sulfur disproportionation in the Mesoproterozoic, *Science*, 310, 1477–1479, 2005.
- Johnston, D. T., Farquhar, J., Habicht, K. S., and Canfield, D. E.: Sulphur isotopes and the search for life: strategies for identifying sulphur metabolisms in the rock record and beyond, *Geobiology*, 6, 425–435, 2008.
- Jones, B. A., Facchetti, A., Wasielewski, M. R., and Marks, T. J.: Theory of oxidation-reduction reactions involving electron transfer. 5. Comparison and properties of electrochemical and chemical rate constants, *J. Am. Chem. Soc.*, 129, 15259–15278, 2007.
- Jørgensen, B. B.: Mineralization of organic matter in the sea bed – the role of sulphate reduction, *Nature*, 296, 643–645, 1982.
- Jørgensen, B. B. and Cohen, Y.: Solar Lake (Sinai), 5. The sulfur cycle of the benthic cyanobacterial mats, *Limnol. Oceanogr.*, 22, 657–666, 1977.
- Kah, L. C., Lyons, T. W., and Frank, T. D.: Low marine sulphate and protracted oxygenation of the Proterozoic biosphere, *Nature*, 431, 834–838, 2004.
- Kampschulte, A. and Strauss, H.: The sulfur isotopic evolution of Phanerozoic seawater based on the analysis of structurally substituted sulfate in carbonates, *Chem. Geol.*, 204, 255–286, 2004.
- Kamysny, A., Jr., Zerkle, A. L., Mansaray, Z. F., Ciglenečki, I., Bura-Nakić, E., Farquhar, J., and Ferdelman, T. G.: Biogeochemical sulfur cycling in the water column of a shallow stratified seawater lake: speciation and quadruple sulfur isotope composition, *Mar. Geol.*, 127, 144–154, 2011.
- Kaplan, I. R. and Rittenberg, S. C.: Microbiological fractionation of sulphur isotopes, *J. Gen. Microbiol.*, 34, 195–212, 1964.
- Kaplan, I. R.: Stable isotopes of sulfur, nitrogen and deuterium in Recent marine environments, in: *Stable Isotopes in Sedimentary Geology*, edited by: Arthur, M. A., Anderson, T. F., Kaplan, I. R., Veizer, J. and Land, L. S., Society for Sedimentary Geology, Tulsa, Oklahoma, 21–108, 1983.
- Kaplan, I. R., Emery, K. O., and Rittenberg, S. C.: The distribution and isotopic abundance of sulphur in recent marine sediments off southern California, *Geochim. Cosmochim. Ac.*, 27, 297–331, 1963.
- Karcz, P.: Relationships between development of organic-rich shallow shelf facies and variation in isotopic composition of pyrite (Middle Triassic, Spitsbergen), *Polish Polar Res.*, 31, 239–254, 2010.
- Karube, Z., Okada, N., and Tayasu, I.: Sulfur stable isotope signature identifies the source of reduced sulfur in benthic communities in macrophyte zones of Lake Biwa, Japan, *Limnology*, 13, 269–280, 2012.
- Kemp, A. L. W. and Thode, H. G.: The mechanism of the bacterial reduction of sulphate and sulphite from isotope fractionation studies, *Geochim. Cosmochim. Ac.*, 32, 71–91, 1968.
- Kleikemper, J., Schroth, M. H., Bernasconi, S. M., Brunner, B., and Zeyer, J.: Sulfur isotope fractionation during growth of sulfate-reducing bacteria on various carbon sources, *Geochim. Cosmochim. Ac.*, 68, 4891–4904, 2004.
- Ku, T. C. W., Walter, L. M., Coleman, M. L., Blake, R. E., and Martini, A. M.: Coupling between sulfur recycling and syndepositional carbonate dissolution: evidence from oxygen and sulfur isotope composition of pore water sulfate, South Florida Platform, USA, *Geochim. Cosmochim. Ac.*, 63, 2529–2546, 1999.
- Kump, L. R. and Arthur, M. A.: Interpreting carbon-isotope excursions: carbonates and organic matter, *Chem. Geol.*, 161, 181–198, 1999.
- Kurtz, A. C., Kump, L. R., Arthur, M. A., Zachos, J. C., and Paytan, A.: Early Cenozoic decoupling of the global carbon and sulfur cycles, *Paleoceanography*, 18, PA000908, doi:10.1029/2003PA000908, 2003.
- Leavitt, W. D., Halevy, I., Bradley, A. S., and Johnston, D. T.: Influence of sulfate reduction rates on the Phanerozoic sulfur isotope record, *Proc. Nat. Acad. Sci. (USA)*, 110, 11244–11249, 2013.
- Lee, Y. J. and Lwiza, K.: Interannual variability of temperature and salinity in shallow water: Long Island Sound, New York, *J. Geophys. Res.*, 110, C09022, doi:10.1029/2004JC002507, 2005.
- Lein, A. Y.: Biogeochemistry of the anaerobic diagenesis of Recent Baltic Sea sediments, *Environ. Biogeochem.*, 35, 441–461, 1983.
- Li, C., Love, G. D., Lyons, T. W., Fike, D. A., Sessions, A. L., and Chu, X.: A stratified redox model for the Ediacaran ocean, *Science*, 328, 80–83, 2010.
- Li, X., Gilhooly, W. P., III, Zerkle, A. L., Lyons, T. W., Farquhar, J., Werne, J. P., Varela, R., and Scranton, M. I.: Stable sulfur isotopes in the water column of the Cariaco Basin, *Geochim. Cosmochim. Ac.*, 74, 6764–6778, 2010.
- Llobet-Brossa, E., Rabus, R., Böttcher, M. E., Könneke, M., Finke, N., Schramm, A., Meyer, R. L., Gröttschel, S., Rosselló-Mora, R., and Amann, R.: Community structure and activity of sulfate-reducing bacteria in an intertidal surface sediment: a multi-method approach, *Aquat. Microbial Ecol.*, 29, 211–226, 2002.
- Lojen, S., Ogrinc, N., Dolenc, T., Vokal, B., Szaran, J., Mihelčić, G., and Branica, M.: Nutrient fluxes and sulfur cycling in the organic-rich sediment of Makirina Bay (Central Dalmatia, Croatia), *Sci. Total Environ.*, 327, 265–284, 2004.
- Lowenstein, T. K., Hardie, L. A., Timofeeff, M. N., and Demicco, R. V.: Secular variation in seawater chemistry and the origin of calcium chloride basinal brines, *Geology*, 31, 857–860, 2003.
- Lowenstein, T. K., Timofeeff, M. N., Kovalevych, V. M., and Horita, J.: The major-ion composition of Permian seawater, *Geochim. Cosmochim. Ac.*, 69, 1701–1719, 2005.
- Loyd, S. J., Marengo, P. J., Hagadorn, J. W., Lyons, T. W., Kaufman, A. J., Sour-Tovar, F., and Corsetti, F. A.: Sustained low marine sulfate concentrations from the Neoproterozoic to the Cambrian: insights from carbonates of northwestern Mexico and eastern California, *Earth Planet. Sci. Lett.*, 339/340, 79–94, 2012.
- Loyd, S. J., Marengo, P. J., Hagadorn, J. W., Lyons, T. W., Kaufman, A. J., Sour-Tovar, F., and Corsetti, F. A.: Local $\delta^{34}\text{S}$ variability in ~580 Ma carbonates of northwestern Mexico and the Neoproterozoic marine sulfate reservoir, *Precamb. Res.*, 224, 551–569, 2013.

- Luo, G. M., Kump, L. R., Wang, Y., Tong, J., Arthur, M. A., Yang, H., Huang, J., Yin, H., and Xie, S.: Isotopic evidence for an anomalously low oceanic sulphate concentration following end-Permian mass extinction, *Earth Planet. Sci. Lett.*, 300, 101–111, 2010.
- Luo, G. M., Ono, S., Algeo, T. J., Huang, J., Li, C., Zhou, L., Liu, J., and Xie, S.C.: Return of Archean low oceanic sulfate levels during the earliest Mesoproterozoic, *Precamb. Res.*, 258, 36–47, 2015.
- Lyons, T. W.: Sulfur isotopic trends and pathways of iron sulfide formation in upper Holocene sediments of the anoxic Black Sea, *Geochim. Cosmochim. Ac.*, 61, 3367–3382, 1997.
- Lyons, T. W. and Gill, B. C.: Ancient sulfur cycling and oxygenation of the early biosphere, *Elements*, 6, 93–99, 2010.
- Lyons, T. W. and Severmann, S.: A critical look at iron paleoredox proxies: New insights from modern euxinic marine basins, *Geochim. Cosmochim. Ac.*, 70, 5698–5722, 2006.
- Mandernack, K. W., Lynch, L., Krouse, H. R., and Morgan, M. D.: Sulfur cycling in wetland peat of the New Jersey Pinelands and its effect on stream water chemistry, *Geochim. Cosmochim. Ac.*, 64, 3949–3964, 2000.
- Mandernack, K. W., Krouse, H. R., and Skei, J. M.: A stable sulfur and oxygen isotopic investigation of sulfur cycling in an anoxic marine basin, Framvaren Fjord, Norway, *Chem. Geol.*, 195, 181–200, 2003.
- Matrosov, A. G., Chebotarev, Y. N., Kudryavtseva, A. J., Zyukun, A. M., and Ivanov, M. V.: Sulfur isotope composition in freshwater lakes containing H₂S, *Geochem. Int.*, 12, 217–221, 1975.
- Mayer, B. and Schwark, L.: A 15,000-year stable isotope record from sediments of Lake Steisslingen, southwest Germany, *Chem. Geol.*, 161, 315–337, 1999.
- McArthur, J. M., Donovan, D. T., Thirlwall, M. F., Fouke, B. W., and Matthey, D.: Strontium isotope profile of the early Toarcian (Jurassic) oceanic anoxic event, the duration of ammonite biozones, and belmenite palaeotemperatures, *Earth Planet. Sci. Lett.*, 179, 269–285, 2000.
- McFadden, K. A., Huang, J., Chu, X., Jiang, G., Kaufman, A. J., Zhou, C., Yuan, X., and Xiao, S.: Pulsed oxidation and biological evolution in the Ediacaran Doushantuo Formation, *Proc. Nat. Acad. Sci. (USA)*, 105, 3197–3202, 2008.
- Millero, F. J.: *Chemical Oceanography*, 3rd Edn., CRC Press, Boca Raton, Florida, 2005.
- Montañez, I. P., Norris, R. D., Algeo, T. J., Chandler, M. A., Johnson, K. R., Kennedy, M. J., Kent, D. V., Kiehl, J. T., Kump, L. R., Ravelo, A. C., and Turekian, K. K.: Understanding Earth's Deep Past: Lessons for Our Climate Future, National Academy of Sciences Press, Washington, DC, 2011.
- Nakagawa, M., Ueno, Y., Hattori, S., Umemura, M., Yagi, A., Takai, K., Koba, K., Sasaki, Y., Makabe, A., and Yoshida, N.: Seasonal change in microbial sulfur cycling in monomictic Lake Fukamiike, Japan, *Limnol. Oceanogr.*, 57, 974–988, 2012.
- Nakai, N. and Jensen, M. L.: The kinetic isotope effect in the bacterial reduction and oxidation of sulfur, *Geochim. Cosmochim. Ac.*, 28, 1893–1912, 1964.
- Nakai, N., Wada, H., Kiyosu, Y., and Takimoto, M.: Stable isotope studies on the origin and geological history of water and salts in the Lake Vanda area, Antarctica, *Geochem. J.*, 9, 7–24, 1975.
- Nakano, T., Tayasu, I., Yamada, Y., Hosono, T., Igeta, A., Hyodo, F., Ando, A., Saitoh, Y., Tanaka, T., Wada, E., and Yachi, S.: Effect of agriculture on water quality of Lake Biwa tributaries, Japan, *Sci. Total Environ.*, 389, 132–148, 2008.
- Newton, R. J., Reeves, E. P., Kafousia, N., Wignall, P. B., Bottrell, S. H., and Sha, J.-G.: Low marine sulfate concentrations and the isolation of the European epicontinental sea during the Early Jurassic, *Geology*, 39, 7–10, 2011.
- Nriagu, J. O. and Coker, R. D.: Emission of sulfur from Lake Ontario sediments, *Limnol. Oceanogr.*, 21, 485–489, 1976.
- Nriagu, J. O. and Harvey, H. H.: Isotopic variation as an index of sulfur pollution in lakes around Sudbury, Ontario, *Nature*, 273, 223–224, 1978.
- Nriagu, J. O. and Soon, Y. K.: Distribution and isotopic composition of sulfur in lake sediments of northern Ontario, *Geochim. Cosmochim. Ac.*, 49, 823–834, 1985.
- Oren, A.: Bioenergetic aspects of halophilism, *Microbiol. Mol. Biol. Rev.*, 63, 334–348, 1999.
- Overmann, J., Beatty, J. T., Krouse, H. R., and Hall, K. J.: The sulfur cycle in the chemocline of a meromictic salt lake, *Limnol. Oceanogr.*, 41, 147–156, 1996.
- Owens, J. D., Gill, B. C., Jenkyns, H. C., Bates, S. M., Severmann, S., Kuypers, M. M. M., Woodfine, R. G., and Lyons, T. W.: Sulfur isotopes track the global extent and dynamics of euxinia during Cretaceous Oceanic Anoxic Event 2, *Proc. Nat. Acad. Sci. (USA)*, 110, 18407–18412, 2013.
- Paytan, A., Kastner, M., Campbell, D., and Thieme, M. H.: Sulfur isotopic composition of Cenozoic seawater sulfate, *Science*, 282, 1459–1462, 1998.
- Paytan, A., Kastner, M., Campbell, D., and Thieme, M. H.: Seawater sulfur isotope fluctuations in the Cretaceous, *Science*, 304, 1663–1665, 2004.
- Peterson, B. J. and Howarth, R. W.: Sulfur, carbon, and nitrogen isotopes used to trace organic matter flow in the salt-march estuaries of Sapelo Island, Georgia, *Limnol. Oceanogr.*, 32, 1195–1213, 1987.
- Planavsky, N. J., Bekker, A., Hofmann, A., Owens, J. D., and Lyons, T. W.: Sulfur record of rising and falling marine oxygen and sulfate levels during the Lomagundi event, *Proc. Nat. Acad. Sci. (USA)*, 109, 18300–18305, 2012.
- Price, F. T. and Casagrande, D. J.: Sulfur distribution and isotopic composition in peats from the Okefenokee Swamp, Georgia and the Everglades, Florida, *Internat. J. Coal Geol.*, 17, 1–20, 1991.
- Purdy, K., Hawes, I., Bryant, C. L., Fallick, A. E., and Nedwell, D. B.: Estimates of sulphate reduction rates in Lake Vanda, Antarctica support the proposed recent history of the lake, *Antarct. Sci.*, 13, 393–399, 2001.
- Rees, C. E.: A steady-state model for sulphur isotope fractionation in bacterial reduction processes, *Geochim. Cosmochim. Ac.*, 27, 1141–1162, 1973.
- Rickard, D. T.: Kinetics and mechanism of pyrite formation at low temperatures, *Am. J. Sci.*, 275, 636–652, 1975.
- Ries, J. B., Fike, D. A., Pratt, L. M., Lyons, T. W., and Grotzinger, J. P.: Superheavy pyrite ($\delta^{34}\text{S}_{\text{pyr}} > \delta^{34}\text{S}_{\text{CAS}}$) in the terminal Proterozoic Nama Group, southern Namibia: a consequence of low seawater sulfate at the dawn of life, *Geology*, 37, 743–746, 2009.
- Röhl, H.-J., Schmid-Röhl, A., Oschmann, W., Frimmel, A., and Schwark, L.: The Posidonia Shale (Lower Toarcian) of SW-Germany: an oxygen-depleted ecosystem controlled by sea level and palaeoclimate, *Palaeogeogr. Palaeoclimatol. Palaeoecol.*, 165, 27–52, 2001.

- Rudnicki, M. D., Elderfield, H., and Spiro, B.: Fractionation of sulfur isotopes during bacterial sulfate reduction in deep ocean sediments at elevated temperatures, *Geochim. Cosmochim. Ac.*, 65, 777–789, 2001.
- Scheiderich, K., Zerkle, A. L., Helz, G. R., Farquhar, J., and Walker, R. J.: Molybdenum isotope, multiple sulfur isotope, and redox-sensitive element behavior in early Pleistocene Mediterranean sapropels, *Chem. Geol.*, 279, 134–144, 2010.
- Shen, Y. A., Buick, R., and Canfield, D. E.: Isotopic evidence for microbial sulphate reduction in the early Archaean era, *Nature*, 410, 77–81, 2001.
- Sim, M. S., Bosak, T., and Ono, S. H.: Large sulfur isotope fractionation does not require disproportionation, *Science*, 333, 74–78, 2011a.
- Sim, M. S., Ono, S. H., Donovan, K., Templer, S. P., and Bosak, T.: Effect of electron donors on the fractionation of sulfur isotopes by a marine *Desulfovibrio* sp., *Geochim. Cosmochim. Ac.*, 75, 4244–4259, 2011b.
- Song, H. Y., Tong, J., Algeo, T. J., Song, H. J., Qiu, H., Zhu, Y., Tian, L., Bates, S., Lyons, T. W., Luo, G. M., and Kump, L. R.: Early Triassic seawater sulfate drawdown, *Geochim. Cosmochim. Ac.*, 128, 95–113, 2014.
- Sørensen, K. B. and Canfield, D. E.: Annual fluctuations in sulfur isotope fractionation in the water column of a euxinic marine basin, *Geochim. Cosmochim. Ac.*, 68, 503–515, 2004.
- Stam, M. C., Mason, P. R. D., Pallud, C., and Van Cappellen, P.: Sulfate reducing activity and sulfur isotope fractionation by natural microbial communities in sediments of a hypersaline soda lake (Mono Lake, California), *Chem. Geol.*, 278, 23–30, 2010.
- Sternbeck, J. and Sohlenius, G.: Authigenic sulfide and carbonate mineral formation in Holocene sediments of the Baltic Sea, *Chem. Geol.*, 135, 55–73, 1997.
- Strauss, H.: The isotopic composition of sedimentary sulfur through time. *Palaeogeogr. Palaeoclimatol. Palaeoecol.*, 132, 97–118, 1997.
- Strauss, H.: Geological evolution from isotope proxy signals-sulfur, *Chem. Geol.*, 161, 89–101, 1999.
- Strauss, H.: Sulfur isotopes and the early Archaean sulphur cycle, *Precamb. Res.*, 126, 349–361, 2003.
- Stribling, J. M., Cornwell, J. C., and Currin, C.: Variability of stable sulfur isotopic ratios in *Spartina alterniflora*, *Mar. Ecol. Progr. Ser.*, 166, 73–81, 1998.
- Suits, N. S. and Wilkin, R. T.: Pyrite formation in the water column and sediments of a meromictic lake, *Geology*, 26, 1099–1102, 1998.
- Sweeney, R. E. and Kaplan, I. R.: Stable isotope composition of dissolved sulfate and hydrogen sulfide in the Black Sea, *Mar. Chem.*, 9, 145–152, 1980.
- Valentine, D. L.: Biogeochemistry and microbial ecology of methane oxidation in anoxic environments: a review, *Antonie van Leeuwenhoek*, 81, 271–282, 2002.
- Wacey, D., McLoughlin, N., Whitehouse, M. J., and Kilburn, M. R.: Two coexisting sulfur metabolisms in a ca. 3400 Ma sandstone, *Geology*, 38, 1115–1118, 2010.
- Werne, J. P., Hollander, D. J., Behrens, A., Schaeffer, P., Albrecht, P., and Damsté, J. S. S.: Timing of early diagenetic sulfurization of organic matter: A precursor-product relationship in Holocene sediments of the anoxic Cariaco Basin, Venezuela, *Geochim. Cosmochim. Ac.*, 64, 1741–1751, 2000.
- Werne, J. P., Lyons, T. W., Hollander, D. J., Formolo, M. J., and Damsté, J. S. S.: Reduced sulfur in euxinic sediments of the Cariaco Basin: sulfur isotope constraints on organic sulfur formation, *Chem. Geol.*, 195, 159–179, 2003.
- Werne, J. P., Lyons, T. W., Hollander, D. J., Schouten, S., Hopmans, E. C., and Damsté, J. S. S.: Investigating pathways of diagenetic organic matter sulfurization using compound-specific sulfur isotope analysis, *Geochim. Cosmochim. Ac.*, 72, 3489–3502, 2008.
- Wijsman, J. W. M., Middelburg, J. J., Herman, P. M. J., Böttcher, M. E., and Heip, C. H. R.: Sulfur and iron speciation in surface sediments along the northwestern margin of the Black Sea, *Mar. Chem.*, 74, 261–278, 2001.
- Wilkin, R. T., Barnes, H. L., and Brantley, S. L.: The size distribution of framboidal pyrite in marine sediments: an indicator of redox conditions, *Geochim. Cosmochim. Ac.*, 60, 3897–3912, 1996.
- Wortmann, U. G. and Chernyavsky, B. M.: Effect of evaporite deposition on Early Cretaceous carbon and sulphur cycling, *Nature*, 446, 654–656, 2007.
- Wortmann, U. G. and Paytan, A.: Rapid variability of seawater chemistry over the past 130 million years, *Science*, 337, 334–336, 2012.
- Wortmann, U. G., Bernasconi, S. M., and Böttcher, M. E.: Hyper-sulfidic deep biosphere indicates extreme sulfur isotope fractionation during single-step microbial sulfate reduction, *Geology*, 29, 647–650, 2001.
- Wotte, T., Strauss, H., Fugmann, A., and Garbe-Schönberg, D.: Paired $\delta^{34}\text{S}$ data from carbonate-associated sulfate and chromium-reducible sulfur across the traditional Lower-Middle Cambrian boundary of W-Gondwana, *Geochim. Cosmochim. Ac.*, 85, 228–253, 2012.
- Wu, N., Farquhar, J., Strauss, H., Kim, S.-T., and Canfield, D. E.: Evaluating the S-isotope fractionation associated with Phanerozoic pyrite burial, *Geochim. Cosmochim. Ac.*, 74, 2053–2071, 2010.
- Zaback, D. A. and Pratt, L. M.: Isotopic composition and speciation of sulfur in the Miocene Monterey Formation: Reevaluation of sulfur reactions during early diagenesis in marine environments, *Geochim. Cosmochim. Ac.*, 56, 763–774, 1992.
- Zerkle, A. L., Kamyshny, A., Jr., Kump, L. R., Farquhar, J., Oduro, H., and Arthur, M. A.: Sulfur cycling in a stratified euxinic lake with moderately high sulfate: Constraints from quadrupole S isotopes, *Geochim. Cosmochim. Ac.*, 74, 4953–4970, 2010.
- Zhang, S., Jiang, G., Zhang, J., Song, B., Kennedy, M. J., and Christie-Blick, N.: U-Pb sensitive high-resolution ion microprobe ages from the Doushantuo Formation in south China: constraints on late Neoproterozoic glaciations, *Geology*, 33, 473–476, 2005.
- Zhang, S., Jiang, G., and Han, Y.: The age of the Nantuo Formation and Nantuo glaciation in South China, *Terra Nova*, 20, 289–294, 2008.